From Remotely-Sensed SIF to Ecosystem Structure, Function, and Service: *Part I - Harnessing Theory*

Ying Sun[1, *], Lianhong Gu[2], Jiaming Wen[1], Christiaan van der Tol[3], Albert Porcar-Castell[4], Joanna Joiner[5], Christine Y. Chang[6], Troy Magney[7], Lixin Wang[8], Leiqiu Hu[9], Uwe Rascher[10], Pablo Zarco-Tejada[11], Christopher B. Barrett[12], Jiameng Lai[1], Jimei Han[1], Zhenqi Luo[1]

[1] School of Integrative Plant Science, Soil and Crop Sciences Section, Cornell University, Ithaca, NY, USA.

[2] Environmental Sciences Division and Climate Change Science Institute, Oak Ridge National Laboratory, Oak Ridge, TN, USA

[3] Affiliation Faculty of Geo-Information Science and Earth Observation (ITC), University of Twente, Netherlands

[4] Optics of Photosynthesis Laboratory, Institute for Atmospheric and Earth System Research (INAR)/Forest Sciences, Viikki Plant Science Center (ViPS), University of Helsinki, Helsinki, Finland

[5] National Aeronautics and Space Administration (NASA) Goddard Space Flight Center (GSFC), Greenbelt, MD, USA

[6] US Department of Agriculture, Agricultural Research Service, Adaptive Cropping Systems Laboratory, Beltsville, MD, USA

[7] Department of Plant Sciences, University of California, Davis, Davis, CA, USA

[8] Department of Earth Sciences, Indiana University-Purdue University Indianapolis (IUPUI), Indianapolis, IN, USA

[9] Department of Atmospheric and Earth Science, University of Alabama in Huntsville, AL, USA

[10] Institute of Bio- and Geosciences, Forschungszentrum Jülich GmbH, Jülich, Germany

[11] School of Agriculture and Food (SAF-FVAS) and Faculty of Engineering and Information Technology (IE-FEIT), University of Melbourne, Melbourne, VIC, Australia

[12]Charles H. Dyson School of Applied Economics and Management, Cornell University, Ithaca, NY, USA

[*]Correspondence to: Ying Sun (ys776@cornell.edu)

Abstract

Solar-induced chlorophyll fluorescence (SIF) is a remotely sensed optical signal emitted during the light reactions of photosynthesis. The past two decades have witnessed an explosion in availability of SIF data at increasingly higher spatial and temporal resolutions, sparking applications in diverse research sectors (*e.g.*, ecology, agriculture, hydrology, climate, and socioeconomics). These applications must deal with complexities caused by tremendous variations in scale and the impacts of interacting and superimposing plant physiology and three-dimensional vegetation structure on the emission and scattering of SIF. At present, these complexities have not been overcome. To advance future research, the two companion reviews aim to 1) develop an analytical framework for inferring terrestrial vegetation structures and function that are tied to SIF emission, 2) synthesize progress and identify challenges in SIF research via the lens of multi-sector applications, and 3) map out actionable solutions to tackle these challenges and offer our vision for research priorities over the next 5-10 years based on the proposed analytical framework. This paper is the first of the two companion reviews, and theory-oriented. It introduces a theoretically rigorous yet practically applicable analytical framework. Guided by this framework, we offer theoretical perspectives on three overarching questions: 1) **The forward (mechanism) question** - How are the dynamics of SIF affected by terrestrial ecosystem structure and function? 2) **The inference question**: What aspects of terrestrial ecosystem structure, function, and service can be reliably inferred from remotely sensed SIF and how? 3) **The innovation question**: What innovations are needed to realize the full potential of SIF remote sensing for real-world applications under climate change? The analytical framework elucidates that process complexity must be appreciated in inferring ecosystem structure and functions from the observed SIF emission; this framework can serve as a diagnosis and inference tool for versatile applications across diverse spatial and temporal scales.

1. Introduction

Land plants harvest light energy for photosynthesis with three types of pigments: chlorophyll *a*, chlorophyll *b*, and carotenoids. The light energy harvested by a free pigment is lost, partly radiatively as fluorescence and partly non-radiatively as heat; as a result, the wavelength of emitted fluorescence is longer than that of the photons originally absorbed, a phenomenon known as Stokes shift. Fluorescence is only emitted from the first excited state (S1) as an electron boosted to a higher energy is immediately relaxed to the S1 state by giving off some heat in a process known as internal conversion (Porcar-Castell et al., 2014). In addition to emitting fluorescence, the S1 state can also relax to the ground state (S0) via internal conversion, in which case heat is released, or transition to a long-lasting excited triplet state of chlorophyll via intersystem crossing. Chlorophyll *a* and *b* extracts in ether can emit up to 30% and 15%, respectively, of the absorbed energy as fluorescence (Barber et al., 1989; Latimer et al., 1956). Carotenoids also fluoresce but their quantum yield is several orders of magnitude lower than those of chlorophyll *a* and *b*, and can effectively be considered as non-fluorescent (Hashimoto et

al., 2018). In *vivo*, the fluorescing characteristics of chlorophyll *a* and *b* change drastically. Within the light-harvesting complexes, the excitation energy transfer from chlorophyll *b* to *a* is ultrafast (Bittner et al., 1994), leaving little chance for chlorophyll *b* to fluoresce; as a result, all chlorophyll fluorescence emission from plants can be considered as originating from chlorophyll *a* (denoted as Chl*a*F emission hereafter). More importantly, photochemical and non-photochemical processes controlled by plant physiology compete with Chl*a*F emission, internal conversion, and intersystem crossing for the excitation energy at the S1 state, which can lead to an order of magnitude decrease in the quantum yield of Chl*a*F emission, depending on environmental conditions. Details about the physical mechanisms of Chl*a*F emission can be found in Papageorgiou & Govindjee (2004) and Porcar-Castell et al. (2014).

Chl*a*F emission has no known physiological or ecological use to plants. It is not directly regulated by plants either. The energy lost in Chl*a*F emission is minuscule and has little impact on the energy budget of plants. However, owing to the principle of energy conservation, the dynamics of Chl*a*F emission are always coupled to the dynamics of photochemical and non-photochemical processes that compete for the excitation energy of the S1 state (Gu et al., 2019; Porcar-Castell et al., 2014). Because plants actively regulate photochemical and non-photochemical processes, the dynamics of Chl*a*F emission spontaneously reflect, but are not directly controlled by, these regulations. Furthermore, because these processes have different time constants, it is possible to differentiate their dynamics from the unique temporal patterns of Chl*a*F emission, as shown in the Kautsky effect (Kautsky & Hirsch, 1931; Stirbet & Govindjee, 2011) and Pulse-Amplitude Modulated fluorometry (PAM) (Baker, 2008).

Chl*a*F emission can be excited by either artificial light, which leads to active fluorescence, or sunlight, which leads to passive, Sun- or Solar-Induced chlorophyll Fluorescence (SIF). Both active and passive Chl*a*F emission have a long history of applications in plant science (Papageorgiou & Govindjee, 2004), ecosystem science (Mohammed et al., 2019), and marine biology (Suggett et al., 2010). Because Chl*a*F emission is a spontaneous, unregulated byproduct of the light harvesting process, physiologically interpreting its dynamics is in general not straightforward, even with active Chl*a*F emission at the leaf scale, where the wavelength and intensity of the excitation light can be carefully manipulated.

The past two decades have witnessed a rapid growth in SIF research, spurred by advances in SIF observing capabilities from various platforms. Applications of remotely sensed SIF range from ecological sciences (e.g., Magney et al., 2019; Sun et al., 2017; Porcar-Castell, et al., 2021), to agricultural (e.g., Guan et al., 2016; Guanter et al., 2014), hydrological (Gentine et al., 2019; Zhan et al., 2022), climate feedback (e.g., Mueller et al., 2016), and even socioeconomic studies (Browne et al., 2021) (Fig. 1). However, such applications face tremendous complexities arising not only from the variations in scale (in both time and space) but also from interacting and superimposing plant physiology and three-dimensional (3D) leaf and canopy structure (in both vertical and horizontal dimensions). Intermingling physiology and structure affect Chl*a*F emission and the subsequent scattering/reabsorption at both leaf and canopy scales (Chang et al.,

2021; Magney et al., 2020; Porcar-Castell et al., 2021; Zhao et al., 2016; van Wittenberghe et al., 2015), as well as the anisotropy of at-sensor SIF (depending on sun-canopy-sensor geometry, Joiner et al., 2020). At present, these complexities have not been overcome. Consequently, the "six blind men and the elephant" analogy, which was used to characterize the current understanding of terrestrial carbon cycling by Fisher et al. (2014) is also appropriate for SIF research. Previous studies may have touched different aspects of the "elephant", resulting in mixed conclusions, for example, the linear vs nonlinear relationships between SIF and gross primary production (GPP) (e.g., Damm et al., 2015; Li, Xiao et al., 2018; Pierrat et al., 2022), the sign/strength of the relationship between quantum yields of different energy dissipation pathways (e.g., Martini et al., 2022; Miao et al., 2018), and the practical added-value of SIF in inferring the functioning of natural and agricultural systems (e.g., Cai et al., 2019; Peng et al., 2020; Sloat et al., 2021; Smith et al., 2018; Wang et al., 2019).

As SIF research progresses, more aspects of the "elephant" should be touched and understood. There is a critical need to connect these different aspects, and perhaps more importantly, to know what key aspects have not been touched yet, before we can predict what the whole "elephant" looks like. To advance, we must harness advances/innovations in theory and data (Fig. 1), in order to shift from correlational analyses to causal quantification and reasoning. Towards this end, we offer our perspectives on critical research priorities moving forward, from the theoretical and observational aspects in two companion reviews (i.e., this paper, and Sun et al., 2023b, respectively). Addressing these priorities will ultimately help improve predictive understanding and management of natural and agricultural ecosystems to enhance the services they offer to society (details in the companion review, Sun et al., 2023b).

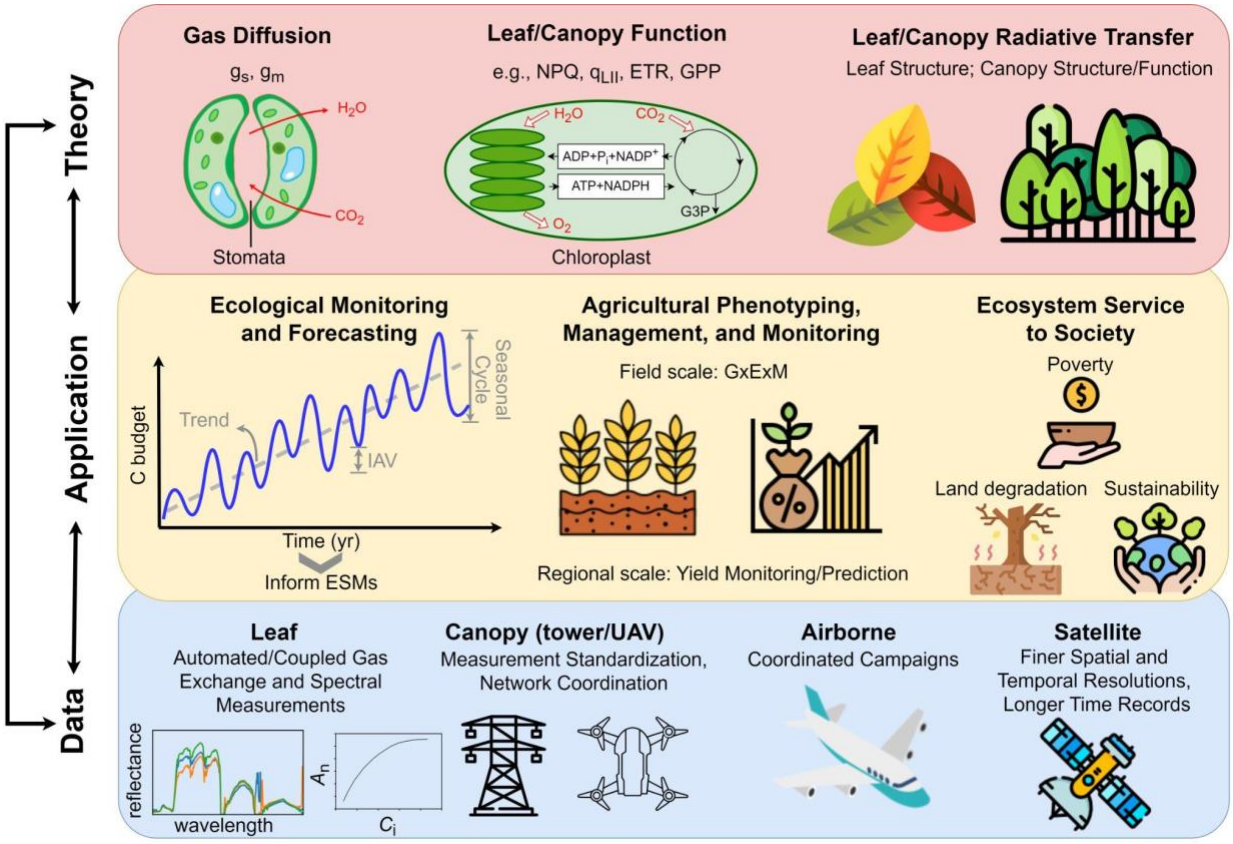

Fig. 1. Harnessing theory and data to enable applications across sectors and scales. Definition of acronyms: GxExM, interactions of Genetics, Environment, and Management; ESMs, Earth System Models; IAV, interannual variability; UAV, Unmanned Aerial Vehicles; ETR, electron transport rate; GPP, Gross Primary Production. Other symbols are defined in Table S1. Icon/images in this diagram come from https://www.flaticon.com/.

The objectives of the two companion reviews are to: 1) develop an analytical framework for inferring terrestrial vegetation structure and functions from remotely-sensed SIF observations, 2) synthesize progress and identify challenges in SIF research through the lens of multi-sector applications, and 3) map out actionable solutions to tackle these challenges and offer our vision for research priorities over the next 5-10 years based on the developed analytical framework. There have been multiple recent reviews of SIF science and applications. For example, Mohammed et al. (2019) provided a historical view of the progress in SIF research since the first discovery of Chl*a*F emission. The reviews of Pacheco-Labrador et al. (2019), Aasen et al. (2019), and Cendrero-Mateo et al. (2019) concentrated on instrumental characteristics, measurement protocols, and retrieval methods for proximal sensing of SIF. The reviews of Porcar-Castell et al. (2014) and Porcar-Castell et al. (2021) provide an introduction of mechanisms that connect SIF to photosynthesis across scales, and present a brief overview of present challenges and unfolding opportunities. They were intended as a first primer on SIF for less advanced audiences and purposefully more qualitative. Compared to these previous reviews, the major contribution of these two companion reviews is to offer a quantitative framework (i.e.,

the theoretical perspective) and a data perspective that can 1) facilitate process interpretation, 2) reconcile contradictory findings reported in literature, and 3) map out concrete future steps (by guiding observational and applicational innovations) to overcome the most pressing challenges towards realizing the full potential of SIF in the broad context of global change biology applications (beyond photosynthesis). Nevertheless, the presence of these reviews not only sets the basis for the present two reviews but also considerably reduces the scope and topics that need to be covered. Throughout the two companion reviews, we emphasize that theory and observations should go hand-in-hand to enable meaningful applications. Both reviews are organized around three overarching questions:

1. **The forward (mechanism) question**: How are the dynamics of SIF affected by terrestrial ecosystem structure and function?
2. **The inference question**: What aspects of terrestrial ecosystem structure, function, and service can be reliably inferred from remotely sensed SIF and how?
3. **The innovation question**: What innovations are needed to realize the full potential of SIF remote sensing for real-world applications under climate change?

The **forward** question concerns mechanisms (i.e., ecosystem structure and functions) that control the emission, reabsorption, and scattering of SIF. It lays the foundation for the next two overarching questions. The **inference** question presents the retrieval of ecosystem structural and functional information from remotely-sensed SIF as an inversion problem, and discusses how such inferred knowledge can inform diverse applications in ecological, agricultural, hydrological, and socioeconomic sectors across scales in time and space. Through the presentation of this inversion problem, we identify knowledge gaps and challenges. Collectively, the answers to the forward and inference questions naturally lead to the **innovation** question, where we propose strategies, solutions, and priorities to fill the knowledge gaps and to overcome present challenges towards maximizing the capability of remotely-sensed SIF to monitor/predict ecosystem structure, function, and service under climate change.

The present paper is the first of the two companion reviews, and theory-oriented. In this paper, we introduce a theoretically rigorous yet practically applicable analytical framework for SIF research. This analytical framework is built upon the rapidly advancing understanding of diverse physiological/structural processes affecting Chl*a*F emission and its subsequent scattering/reabsorption within a canopy. Necessary assumptions/simplifications made in this conceptualization are explicitly stated for future studies to refine. Such an analytical framework is arguably the most critical research priority moving forward, as it enables explicitly elucidating the "causal" relationships/connections among different aspects of the "elephant", and making the knowledge gaps/challenges identified for SIF research tractable and quantifiable. Note that the present review focuses on mechanistic understanding and is rather theoretical and quantitative, readers who are just starting SIF research are advised to first read earlier reviews, particularly Porcar-Castell et al. (2014), Mohammed et al. (2019), and Porcar-Castell et al. (2021).

2. The forward question: How are the dynamics of SIF affected by terrestrial ecosystem structure and function?

The forward question concerns understanding and modeling the absorption of PAR (Photosynthetically Active Radiation, i.e., the excitation photons), subsequent Chl*a*F emission, and its scattering and reabsorption along the path to the sensor in a complex structure of leaf and canopy. Photosynthesis is typically separated into the light and carbon reactions. Issues related to the Chl*a*F emission can be more clearly discussed if we further separate the light reactions into the *photophysical* and *photochemical* reactions (Kamen 1963). The photophysical reactions cover the light harvesting and partitioning between photosystems, excitation energy transfer and trapping, and partitioning of excitation energy into different dissipation pathways. The photochemical reactions include the water splitting by the oxygen evolving complex, the electron transport from PSII to the cytochrome b6f complex (Cyt) to PSI to the eventual acceptor NADP+ with plastoquinone, plastocyanin, and ferredoxin as electron carriers, and the associated proton transport from stroma to lumen and ATP synthesis. The carbon reactions refer to the downstream processes in photosynthesis, i.e., the Calvin-Benson cycle, and are typically modeled by *biochemical* models, such as the Farquhar-von Caemmerer-Berry (FvCB) model (Farquhar et al., 1980). The Chl*a*F emission occurs during the light reactions, more specifically during the photophysical reactions. The value of SIF as a photophysical variable lies in its potential for providing information related to photochemical and biochemical variables.

2.1 Theoretical basis

Theoretically, the total irradiance of Chl*a*F emission at wavelength λ_F (nm, ranging from 640 to 850nm) by a homogeneous canopy with total leaf area index (LAI, m^2 leaf area m^{-2} ground area), denoted as $F_{eT}(\lambda_F)$ (µmol photons m^{-2} ground area s^{-1} nm^{-1}), without considering any scattering and reabsorption by the canopy, can be described as:

$$F_{eT}(\lambda_F) = \int_0^{LAI} F_e(L,\lambda_F)dL$$
$$= \int_0^{LAI} p(L) \int_{\lambda_{Imin}}^{\lambda_F} \{\underbrace{\Phi_{FII}(L)s_{II}(\lambda_F)\beta(L,\lambda_I)}_{\text{PSII}} + \underbrace{\Phi_{FI}(L)s_I(\lambda_F)[1-\beta(L,\lambda_I)]}_{\text{PSI}}\}\sigma(L,\lambda_I)I(L,\lambda_I)d\lambda_I dL \quad (1)$$

Here F_e denotes the Chl*a*F emission of an infinitely thin leaf layer with a thickness of dL at the canopy depth L and emission wavelength λ_F, and is contributed by two components - Chl*a*F emission from photosystem II and I (denoted as PSII and PSI hereafter). The need to include both PSII and PSI contributions is discussed in detail in SI-1. At the leaf level, the F_e component arising from PSII can be represented as the product of the broadband fluorescence quantum yield of PSII (Φ_{FII}, unitless), the total concentration (p, mol m^{-2} leaf area) of light-harvesting photosynthetic pigments (i.e., chlorophyll *a* and *b*, and carotenoids) associated with PSII (i.e., $p \cdot \beta$, where β is the fraction of $p$associated with PSII), the fluorescence spectral shape function s_{II} (unitless), the overall effective absorption cross section of photosynthetic pigment (σ, m^2 mol^{-1}, which may vary with leaf and canopy structure), and the excitation irradiance I (µmol photons m^{-2} leaf area s^{-1} nm^{-1}), which is in turn integrated over the spectra of excitation irradiance wavelength λ_I (nm) from λ_{Imin} (the minimum wavelength of excitation irradiance) up

to λ_F. The excitation photons at λ_I greater than λ_F cannot contribute to F_e at λ_F, as they do not have sufficient energy for Chl*a*F emission at shorter wavelengths (phonon emission due to elementary excitation is ignored as it is non-significant to Chl*a*F emission). Note that I includes all sources - incoming solar photons (i.e., the first-order interaction), scattered solar photons, and emitted fluorescence photons, although contribution from the latter two sources to F_e is considerably smaller (Yang & van der Tol, 2018). The F_e component arising from PSI can be similarly modeled, except that the relative contribution of pigments associated with PSI to the overall effective absorption cross section is denoted as $1-\beta$ (assuming there are no free energetically disconnected light harvesting complexes). The product of p and σ gives the more commonly used absorption coefficient α at the leaf level (unitless, ~0.85 of PAR). Here Φ_{FII} and Φ_{FI} are broadband quantities assumed to be independent of λ_F and λ_I. s_{II} and s_I depend on the electronic properties of the chlorophyll *a* forms involved in the Chl*a*F emissions of PSII and PSI respectively, and their interactions with macromolecular complexes; they lead to unity once integrated over the full range of λ_F, and for simplicity, are assumed to vary only with λ_F.

The leaf-level F_e, once summed up with contributions from PSII and PSI, can be integrated over the full canopy, from the canopy top (i.e., canopy depth $L=0$) to the bottom ($L=LAI$), to obtain the true canopy-level total Chl*a*F emission F_{eT} (i.e., prior to reabsorption or scattering within a canopy). Here the leaf to canopy integration $\int_0^{LAI}$ is a highly conceptualized notation, and can take different forms with varying complexity in actual implementations, i.e., 1D homogeneous (Van der Tol et al., 2009), or 3D heterogeneous canopies (Zhao et al., 2016), or separated sunlit and shaded canopies (e.g., He et al., 2017).

In practice, however, F_{eT} cannot be measured directly. Instead, the canopy-leaving SIF irradiance that travels towards the sensor direction is only a portion of F_{eT} that escapes from the canopy (after reabsorption and scattering). At the nadir view, $F_\uparrow(\lambda_F)$ and $F_\downarrow(\lambda_F)$ (μmol photons m^{-2} ground area s^{-1} nm^{-1}), denoting the upward and downward canopy-leaving SIF irradiance at λ_F within a hemispherical 180° field of view (FOV) at the top and the bottom of a canopy respectively, can be given as:

$$\begin{cases} F_\uparrow(\lambda_F) \\ = \overbrace{\int_0^{LAI} p(L)\varepsilon_\uparrow(L,\lambda_F)\int_{\lambda_{Imin}}^{\lambda_F}\{\underbrace{\Phi_{FII}(L)s_{II}(\lambda_F)\beta(L,\lambda_I)}_{\text{PSII}}+\underbrace{\Phi_{FI}(L)s_I(\lambda_F)[1-\beta(L,\lambda_I)]}_{\text{PSI}}\}\sigma(L,\lambda_I)I(L,\lambda_I)d\lambda_I dL}^{\text{Canopy}} \\ +\overbrace{\varepsilon_\uparrow(LAI,\lambda_F)r_s(\lambda_F)F_\downarrow(\lambda_F)}^{\text{Soil}} \qquad \text{(a)} \\ \\ F_\downarrow(\lambda_F) \\ = \int_0^{LAI} p(L)\varepsilon_\downarrow(L,\lambda_F)\int_{\lambda_{Imin}}^{\lambda_F}\{\underbrace{\Phi_{FII}(L)s_{II}(\lambda_F)\beta(L,\lambda_I)}_{\text{PSII}}+\underbrace{\Phi_{FI}(L)s_I(\lambda_F)[1-\beta(L,\lambda_I)]}_{\text{PSI}}\}\sigma(L,\lambda_I)I(L,\lambda_I)d\lambda_I dL \qquad \text{(b)} \end{cases} \tag{2}$$

$F_{\uparrow}$ consists of a dominant component directly from vegetation (i.e., F_{eT} escaped from the canopy in the upward direction) and a minor component due to reflection of $F_{\downarrow}$ by soil with a reflectance of r_s at λ_F. The major differences of $F_{\uparrow}$ and $F_{\downarrow}$ from F_{eT} are the introduction of the upward and downward escape probabilities, denoted by $\varepsilon_{\uparrow}$ and $\varepsilon_{\downarrow}$ (unitless), respectively, both of which vary with L and λ_F. Any SIF photon emitted by an infinitely thin layer at canopy depth L can be either absorbed 1) by this thin layer, 2) by the part of the canopy above this thin layer, 3) by the part of the canopy below this thin layer, or escape to the 4) very top or 5) very bottom of the canopy. The upward canopy escape probability $\varepsilon_{\uparrow}$ is the probability of a SIF photon emitted at a canopy depth L escaping to the very top of the canopy whereas the downward canopy escape probability $\varepsilon_{\downarrow}$ is the probability of this SIF photon escaping to the very bottom of the canopy. These two probabilities change in reverse directions with L; for example, as L increases, $\varepsilon_{\uparrow}$ decreases while $\varepsilon_{\downarrow}$ increases. Note they are not the same as the probabilities of a SIF photon escaping from the interior to the surface of the same leaf at L. $\varepsilon_{\uparrow}$, $\varepsilon_{\downarrow}$, and the self-absorption probability by the whole canopy ε_{α} sum to unity. As the SIF signal is usually acquired from instruments above the canopy, we further remove the explicit appearance of $F_{\downarrow}$ in Eq 2a, by inserting Eq 2b and obtain:

$$F_{\uparrow}(\lambda_F) = \int_0^{LAI} p(L)[\varepsilon_{\uparrow}(L,\lambda_F) + \varepsilon_{\uparrow}(LAI,\lambda_F)\varepsilon_{\downarrow}(L,\lambda_F)r_s(\lambda_F)]$$

$$\int_{\lambda_{Imin}}^{\lambda_F} \{\underbrace{\Phi_{FII}(L)s_{II}(\lambda_F)\beta(L,\lambda_I)}_{\text{PSII}} + \underbrace{\Phi_{FI}(L)s_I(\lambda_F)[1-\beta(L,\lambda_I)]}_{\text{PSI}}\}\sigma(L,\lambda_I)I(L,\lambda_I)d\lambda_I dL \quad (2c)$$

Eq 2 is also a conceptualized framework and includes necessary simplifications. For example, it omits multiple scattering of SIF within the canopy and by soil (as $\varepsilon_{\uparrow}$ and $\varepsilon_{\downarrow}$ only represent the first-interaction), as well as the backward scattering of SIF from the sky; it also assumes that all photons (in the PAR region) are equally efficient in exciting chlorophylls regardless of wavelength (i.e., Φ_{FII} and Φ_{FI} are broadband quantities). For more technical treatments of excitation and radiative transfer of SIF, readers are referred to Pedrós et al. (2010) and Vilfan et al. (2016) for leaf-level radiative transfer model (RTM), and Van der Tol et al. (2009), Verhoef (1984), van der Tol et al. (2019) for canopy-level 1D RTM, as well as references synthesized in Table 1. Towards achieving objectives of this review, Eq 2c is sufficiently detailed and serves as the base equation for describing SIF dynamics at the canopy scale (and beyond) throughout the rest of the paper. Note the commonly used terminology "SIF remotely sensed above the canopy" corresponds to $F_{\uparrow}$ (if the sensor has an approximately hemispherical 180° FOV) or directional $F_{\Omega\uparrow}$(if the sensor has a narrow FOV; here the sun-canopy-sensor geometry is denoted as $\Omega\uparrow$ in the upward direction, e.g., for spaceborne instruments). The complete formulation of $F_{\Omega\uparrow}$ is provided in SI-2. For simplicity, the following equations and derivations, are all based on $F_{\uparrow}$ unless otherwise specified, but $F_{\Omega\uparrow}$ and $F_{\uparrow}$ are mutually convertible (3.1); plant structural and functional variations as well as environmental forcings that impact $F_{\uparrow}$ (2.2 and 2.3) also apply to $F_{\Omega\uparrow}$.

We further expand Φ_{FII} and Φ_{FI} in Eq 2c as functions of non-photochemical quenching (NPQ) and redox states of PSII and PSI (full derivation in SI-3):

$$F_{\uparrow}(\lambda_F) = \int_0^{LAI} \frac{p(L)[\varepsilon_{\uparrow}(L,\lambda_F) + \varepsilon_{\uparrow}(LAI,\lambda_F)\varepsilon_{\downarrow}(L,\lambda_F)r_s(\lambda_F)]}{1+k_{DF}}$$

$$\int_{\lambda_{Imin}}^{\lambda_F} \left\{ \underbrace{\frac{(1-\Phi_{PSIIm})s_{II}(\lambda_F)\beta(L,\lambda_I)}{[1+NPQ(L)](1-\Phi_{PSIIm})+q_{LII}(L)\Phi_{PSIIm}}}_{\text{PSII}} + \underbrace{\frac{(1-\Phi_{PSIm})s_I(\lambda_F)[1-\beta(L,\lambda_I)]}{[1+q_7(L)NPQ_7](1-\Phi_{PSIm})+q_{LI}(L)\Phi_{PSIm}}}_{\text{PSI}} \right\} \sigma(L,\lambda_I)I(L,\lambda_I)d\lambda_I dL \quad (3)$$

Here q_{LII} and q_{LI} (unitless) denote the fraction of open PSII and PSI reaction centers (characterizing their redox states respectively) under the lake model of photosynthetic unit connectivity, respectively. q_7 is the oxidized fraction of PSI electron donor $P700^+$, an efficient non-photochemical quencher whose intrinsic thermal dissipation capacity is denoted as NPQ_7 (unitless). Φ_{PSIIm} and Φ_{PSIm} (unitless) are the maximal photochemical quantum yields for PSII and PSI, respectively, and assumed to be conserved across non-stressed plants (Björkman & Demmig, 1987; G. N. Johnson et al., 1993). k_{DF} (unitless) is the ratio of k_D (the rate constant of the constitutive or unregulated heat dissipation) to k_F (the rate constant of the Chl*a*F emission). A complete list of variable definitions and units is provided in Table S1.

Eq 3 maps the complex dynamics of the emission and radiative transfer of SIF into a quantitative framework to infer ecosystem structure and functions (Fig. 2). Here Φ_{PSIIm},Φ_{PSIm}, k_{DF}, NPQ_7, s_{II} and s_I can be treated as parameter constants (i.e., invariants in time and possibly across species, detailed discussion in SI-4). The remaining quantities are dynamic variables (i.e., changing over time and across species) and are affected by a myriad of interactive processes encompassing leaf and canopy structure and functions, all of which are driven by ambient environmental forcings (Fig. 2). Although Eq 3 and Fig. 2 show the complexity and challenges of interpreting remotely-sensed SIF, they reveal ***why*** SIF is useful and ***how*** to conduct ecologically meaningful applications of SIF across scales in time and space.

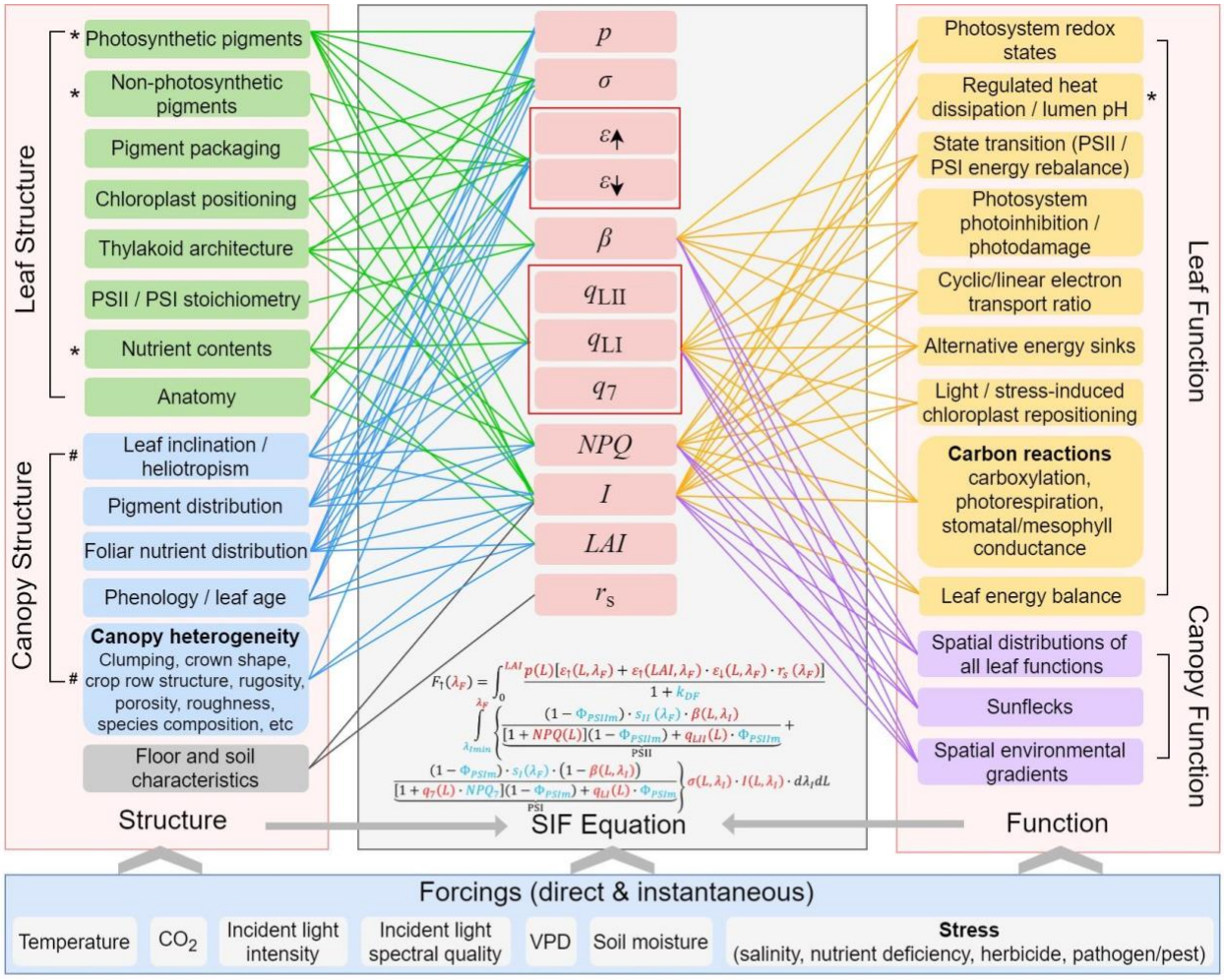

Fig. 2. Diagram mapping key leaf/canopy structure/functions to the full SIF equation (Eq 3). For visualization clarity, only direct effects, which act via first-order processes, are displayed (as linkages between processes and mathematical terms). Boxes marked with * or # highlight processes that can potentially be inferred from hyperspectral or Lidar measurements, respectively.

2.2 How do leaf and canopy functions influence SIF?

Fig. 2 reveals that NPQ, q_{LII}, q_{LI}, q_7, and β are the direct linkages between plant functions and SIF (the right column), and known to be closely regulated by physiology in response to ambient environmental conditions. Note when italicized, NPQ denotes the variable in equations; when non-italicized, NPQ denotes the regulated heat dissipation processes, following Porcar-Castell et al. (2014). NPQ consists of multiple complex mechanisms *(e.g.*, energy-dependent and energy-

independent/sustained NPQ) that operate at different time scales, ranging from seconds to weeks or even longer durations (Ruban, 2016; Verhoeven, 2014). The energy-dependent NPQ is controlled by changes in lumen acidity, which in turn is determined by protons from water splitting by the oxygen evolving complex and translocation from stroma to lumen as a result of photosynthetic electron transport. The energy-independent/sustained NPQ is caused by photoinhibition or photodamage of PSII and/or composition changes in photosynthetic and non-photosynthetic pigment contents for photoprotection (Malnoë, 2018). These mechanisms play key roles in protecting the photosynthetic machinery by dissipating excess energy into harmless heat when the carbon reactions cannot consume all the energy supplied by the light reactions. The consequence of NPQ is to reduce (quench) Chl*a*F emission. Note throughout the paper, NPQ refers to only PSII unless otherwise specified as in the example of NPQ_7 (detailed discussion in SI-3).

q_{LII} and q_{LI} indicate the redox status of PSII and PSI acceptors, respectively. q_7 indicates the redox state of the donor of PSI, and is relevant because the oxidized donor of PSI is an efficient quencher. These variables affect and also are affected by the electron transport rates (ETR) via these two photosystems (Han, Chang, et al., 2022; Laisk et al., 2014). Changes in q_{LII}, q_{LI}, and q_7 are considered instantaneous (i.e., faster than the energy-dependent NPQ). However, photoinhibition may also affect q_{LII}, leading to long-term (weekly to seasonal) changes (Porcar-Castell, 2011).

β is controlled by PSII/PSI stoichiometry and varies with state transition (which may vary across plant species), which refers to the adjustment of PSII and PSI relative absorption cross sections in response to excitation imbalance between PSII and PSI (Stirbet et al., 2020). Photosystem excitation imbalance can occur when environmental conditions such as light intensity, temperature, and CO_2 concentration vary, causing a need to adjust the relative proportion of cyclic to linear electron transport and the ratio of ATP to NADPH to satisfy different stromal metabolisms and deliver electrons to alternative sinks (Kramer & Evans, 2011). Linear electron transport results in the production of NADPH and accumulation of protons in the lumen and therefore ATP synthesis. In contrast, cyclic electron transport contributes to proton accumulation in the lumen and ATP synthesis but not NADPH. Thus adjusting the ratio of cyclic to linear electron transport results in a different ratio of ATP to NADPH. The photosystem excitation imbalance can also occur when the two photosystems encounter different levels of photodamage or photoinhibition (Caffarri et al., 2014). Note that the excitation balance between PSII and PSI is related to, but different from, the energy supply and demand balance between the light and carbon reactions. The former is concerned about the coordination between PSII and PSI for the production of NADPH and ATP, while the latter is concerned about whether the production of NADPH and ATP is at rates that meet their demand by metabolic processes. Both balances can affect Chl*a*F emission. A detailed discussion on these issues is beyond the scope of this review but can be found in the literature of plant physiology (e.g., Kramer & Evans, 2011).

Here it suffices to state that any environmental factors that affect photosynthesis and photorespiration are expected to affect NPQ, q_{LII}, q_{LI}, q_7, and β and therefore SIF dynamics as Eq. 3 and Fig. 2 show. For example, the ratio of q_{LII} to $1 + NPQ$ is directly related to carbon reactions (Eqs S12, S15, S19, mathematical derivation in SI-5). This indicates that any environmental factor that affects carboxylation, oxygenation, stomatal conductance, mesophyll

conductance, and leaf energy balance has a potential to affect NPQ and q_{LII}, and thus $F_{\uparrow}$ (Han, Gu, et al., 2022).

While the above description shows that a wide range of plant functional factors can affect $F_{\uparrow}$ at the leaf level, all is not lost in complexities. Photochemical and non-photochemical quenching have a compensating effect on Chl*a*F emission and may facilitate the interpretation of SIF dynamics (but may complicate the interpretation of SIF-GPP relationships, detailed discussion Sun et al., 2023b). Under steady state in natural conditions, NPQ and q_{LII} tend to vary in opposite directions because more reduced PSII acceptors tend to be associated with higher proton gradients across the thylakoid membrane and therefore higher NPQ. This means that Φ_{FII} is more stable than either NPQ or q_{LII} alone (Gu et al., 2019). Similarly, q_{LI} and q_7 should also tend to change in opposite directions (i.e., more open PSI reaction centers mean less oxidized PSI donors), which may have implications for quantifying Chl*a*F emissions from PSI (detailed discussion in SI-1).

The aforementioned leaf-level plant functions can vary considerably across the canopy, driven by gradients in micro-environmental conditions (e.g., light, temperature, etc) within a canopy and canopy structure (i.e., heterogeneity of foliar traits such as vertical distributions of nutrients, pigments, morphology, age, etc., details in 2.3) within a canopy. For example, it is well known that foliar nutrient contents and morphological characteristics (e.g., specific leaf area) vary systematically across the depth of the canopy. These vertical gradients in foliar traits are long-term adaptations to the background gradients in environmental conditions such as light intensity, spectral composition, and temperature that exist inside the canopy (Coble et al., 2017). The vertical gradients in the light intensity and its spectral composition can impact relative contributions of PSII and PSI to Chl*a*F emission. Plant canopies not only attenuate light intensity but also alter light spectrum because leaves absorb strongly in blue and red wavelengths but scatter strongly in the green and far-red regions. As a result, the within-canopy light environment is depleted in blue and red photons but enriched in green and far-red lights as compared to that in open environments (Hertel et al., 2011). PSI is more sensitive to far-red light than PSII is. Therefore as the canopy gets deeper, the light environment increasingly favors PSI (Anderson et al., 2008), which may lead to increasing contribution of PSI to $F_{\uparrow}$. Collectively, canopy structure and spatial gradients in environmental conditions together determine the vertical variations in leaf photosynthetic rates, NPQ, q_{LII}, q_{LI}, q_7, β and hence $F_{\uparrow}$.

A particularly interesting but often overlooked issue is how sunflecks affect Chl*a*F emission. Sunflecks are bursts of light intensity inside canopies where the light environment is normally shaded. These bursts are caused by canopy gaps and swinging upper canopies by winds and can affect canopy photosynthesis significantly (Way & Pearcy, 2012). Because sunflecks are short-lived and NPQ is not instantaneous (Kromdijk et al., 2016), NPQ might not be able to rise fast enough to quench fluorescence when a sunfleck hits a leaf. As a result, sunflecks may contribute disproportionately to $F_{\uparrow}$ via a short term (a few seconds) increase (i.e. the Kautsky effect), an issue particularly important for plant breeding towards enhancing crop productivity (Kromdijk et al., 2016).

2.3 How do leaf and canopy structure influence SIF?

The internal structure and morphology of a leaf is as complex as that of a plant canopy. Although leaves typically consist of three main tissues (epidermis, mesophyll, and vascular), how these tissues are internally arranged and by what amount are determined by plant phylogenesis, locations in the canopy, foliar age before full development, and environmental conditions, with consequences on the scattering and absorption of both excitation light and emitted SIF (the left column in Fig. 2).

At the sub-daily time scale, the variation in p amount is likely minor (Wickliff & Aronoff, 1962), and dominated by changes in leaf carotenoid composition, which is involved not only in light harvesting and excitation to chlorophylls but also in the xanthophyll cycle that protects plants against photodamage under high light (Adams & Demmig-Adams, 1992). Although leaf chlorophyll content p is not expected to vary diurnally, chloroplast movement occurs at this time scale, leading to changes in excitation irradiance. At seasonal time scales, leaf chlorophyll *a* and *b* and carotenoid contents (bulk xanthophylls and zeaxanthin retention) can be highly dynamic in response to the environment or plant phenology, especially for non-evergreen species. For example, chlorophyll *a* and *b* are lower in young leaves, peaks in mature leaves, and then decreases again as leaves senesce. This leaf age-related pattern closely matches that of leaf nitrogen content and coordinates with photosynthetic capacity (Croft et al., 2017), ensuring that light harvesting and carboxylation are in balance throughout the lifetime of a leaf. Leaf chlorophyll content also varies markedly across species (e.g., evergreen vs non-evergreen), even at the same geographical/climatic regimes (Li, He, et al., 2018).

The effective absorption cross sections of photosynthetic pigment σ is influenced by multiple leaf/canopy structural factors. For example, photosynthetic pigments are not distributed uniformly on a plane that parallels the leaf surface, because pigments in chloroplast thylakoid membranes form concentrated interconnected complexes (i.e., pigment packaging, which refers to the spatial arrangement of pigment molecules, much like leaf clumping in a canopy) and chloroplasts themselves are not uniformly distributed laterally (i.e., chloroplast positioning), leading to the so-called sieve effect. The sieve effect reduces σ, which is in contrast to the detour effect, which increases photon absorption due to multiple scattering inside leaf tissues (Vogelmann, 1993). Furthermore, leaf anatomy can greatly affect the sieve and detour effects. For example, leaves of most species are dorsiventral with chloroplast-rich palisade parenchyma cells densely packed near the upper surface (the adaxial side) and the spongy mesophyll loosely placed near the lower surface (the abaxial side). The dorsiventral leaves tend to orient more or less randomly around horizontal directions. Leaves that orient more vertically tend to have more symmetrical tissue distributions (*e.g.*, grasses, eucalyptus). Ustin & Jacquemoud (2020) provided an excellent discussion on leaf anatomy in the context of leaf-level radiative transfer. Moreover, σ can vary vertically along the canopy due to changes in leaf inclination, pigment distribution, and leaf age.

The escape probabilities $\varepsilon_{\uparrow}$ and $\varepsilon_{\downarrow}$ for a single leaf depend not only on leaf pigment content and composition, but also on leaf anatomy, incident light direction relative to the leaf surface, and fraction of diffuse light, and is best estimated by a leaf/canopy RTM that treats a

leaf as a 1D or 3D structure. It is important to note that, although the morphological architecture of leaves tends to remain stable once the leaf is fully developed, the arrangement and disposition of photosynthetic elements within a canopy therein can be highly dynamic, even at sub-daily scale. Chloroplast positions in mesophyll cells are controlled by chloroplast actin filaments, which are extremely sensitive to the intensity of light. At low light, these filaments can guide chloroplasts to periclinal walls to maximize exposure to light while at high light they can relocate the chloroplasts to anticlinal walls to reduce light exposure to avoid photodamage (Wada, 2013). Similarly, the arrangement of thylakoids within the chloroplast, with dynamic grana stacking/unstacking will also influence $\varepsilon_{\uparrow}$ and $\varepsilon_{\downarrow}$, and also σ.

Overall, the presence of these factors means the leaf internal light intensity and spectral composition is heterogeneous and dynamic. Also, leaves with the same chlorophyll content may have different $\varepsilon_{\uparrow}$, $\varepsilon_{\downarrow}$, and σ if their anatomy and chlorophyll packaging patterns (both at the scale of chloroplasts and thylakoids) differ.

The effects of canopy structure on SIF are twofold. On the one hand, the internal distribution of PAR over branches, needles, and leaves, which controls the excitation of Chl*a*F emission, is determined by the penetration and scattering of light in the stand. On the other hand, the probability that the Chl*a*F emission, which is produced in the stand and exits the canopy in the viewing direction, is also determined by the vegetation structure and incident light direction (Van der Tol et al., 2009). Thus, the optical properties of soil, wood, and leaves in both the excitation and the emission spectral ranges affect canopy-leaving SIF. Fortunately, there is no new physics involved in the theory of SIF radiative transfer. Our understanding regarding how canopy structure affects radiative transfer of incoming solar radiation (Ross, 1981) can be equally applied to radiative transfer of SIF, although the objectives of applying this theory differ greatly between them. For solar radiative transfer, the source comes down from the top and we are typically interested in how much solar radiation is absorbed and how much is reflected. For fluorescence radiative transfer, the source is every leaf inside the canopy and much weaker, and we are typically interested in how much Chl*a*F emission escapes to the top of the canopy (TOC) and what it can tell us about photochemical and biochemical processes inside the canopy. Because of these differences, it is likely that fluorescence radiative transfer issues will require more accurate considerations of canopy structural factors (leaf inclination/heliotropism, spatial variations in pigment and nutrient contents, phenological stages/leaf age, leaf clumping, crown shape, crop row orientation, canopy rugosity, porosity, roughness, etc., Fig. 2) than modeling solar radiative transfer inside plant canopies. The spatial arrangement of fluorescing and non-fluorescing foliage elements within a canopy may have a large influence on $F_{\uparrow}$. For example, forests may appear 'darker' in terms of $F_{\uparrow}$ than croplands (Colombo et al., 2018), not necessarily because they emit less fluorescence, but because a portion of the Chl*a*F emission remains 'trapped' in the vegetation and is reabsorbed, and thus cannot be observed by the sensor. Progress in SIF RTM of different complexity is summarized in 2.4.

2.4 Forward model parameterization of SIF and the associated processes in leaf/canopy function/structure

Existing models that have SIF-simulating capability and progress made so far are summarized in Table 1. Future theoretical innovations needed are discussed in Section 4. Considering the complexity of interacting processes (i.e., the left and right columns in Fig. 2),

model parameterization can be distilled into a few key variables (i.e., the middle column in Fig. 2). Among these variables, $p$and $LAI$are either input or state variables of a dynamic vegetation growth model; $\sigma$of a leaf and r_s can be simulated by leaf/canopy and soil RTM, respectively, or prescribed as input spectra; β is often treated as a constant, i.e., ~0.5. The remaining quantities have to be explicitly formulated, which can be categorized into two groups: variables related to leaf-level physiological functions including NPQ, q_{LII}, q_{LI}, and q_T, and variables determined by leaf/canopy radiative transfer, including I, $\varepsilon_\uparrow$, $\varepsilon_\downarrow$. All models with SIF-simulating capability have to incorporate both leaf-level physiology of Chl*a*F emission and leaf/canopy RTM of solar radiation and SIF, but to varying degrees of parameterization complexity, computational efficiency, and applicable scales (Table 1).

Leaf-level modeling of Chl*a*F emission: Forward estimation of $F_\uparrow$ requires the dynamic responses of NPQ, q_{LII}, q_{LI}, q_T, and β to be known at each canopy depth, according to Eq 3. To the best of our knowledge, no models have been developed for q_{LI}, q_T, and β, therefore we here focus on NPQ and q_{LII}. NPQ and q_{LII} are routinely measured with PAM fluorometry and can be easily parameterized as an empirical function of environmental conditions (e.g., Han, Chang, et al., 2022; Raczka et al., 2019; Serôdio & Lavaud, 2011; van der Tol et al., 2014). An advantage of such simple models is that they can be coupled directly with Eq 3 to forward-calculate $F_\uparrow$. Kinetic models of NPQ based on its regulation by lumen pH have also been developed (e.g., Zaks et al., 2012). However, the latter models are probably too complex for large-scale applications of SIF as they involve many parameters that cannot be estimated directly at the leaf level. Recently there have been efforts in developing mechanistic closure solutions for NPQ and q_{LII} by modeling redox reactions along the electron transport chain (Gu et al. 2022). These closure solutions will allow NPQ and q_{LII} to be resolved in a coupled system of photophysics, photochemistry, and biochemistry of photosynthesis, as defined above.

Leaf/canopy-level RTM of SIF: The widely employed leaf-level RTM includes FluoMODleaf and Fluspect (Pedrós et al., 2010; Vilfan et al., 2016, 2018). Dorsiventral (Stuckens et al., 2009) or 3D leaf RTM (Govaerts et al., 1996) exist, but these do not include physiological parameterization of Chl*a*F emission. At the canopy scale, FluorSAIL (Miller et al., 2005) and Soil-Canopy Observation of Photochemistry and Energy (SCOPE) (Van der Tol et al., 2009) were the first models to parameterize the absorption of PAR, as well as the Chl*a*F emission, reabsorption, and scattering. These models employ the concept of the Scattering of Arbitrarily Inclined Leaves (SAIL) model (Verhoef, 1984, 1985), a relatively simple stochastic model for inclined leaves in stacked layers, which further extended to SIF radiative transfer. This type of model treats the vegetation canopy as 1D horizontally homogeneous canopy, which is unable to realistically characterize heterogeneous canopies that have complex architecture and species composition. To address this issue, ray-tracing based models were developed to simulate radiative transfer of SIF within 3D canopies. Such types of models, including DART, FluorWPS, FluorFLIGHT, and FLiES (Table 1), are computationally more expensive; however, with Monte-Carlo approaches, their applicability for satellite measurements is foreseeable in the near future (Wang et al. 2022). The recently developed FluorRTER model (Zeng et al., 2020), based on spectral invariant theory, could be suitable for 3D heterogeneous canopies and is computationally less demanding.

Among all these models, the 1D SCOPE model is the most widely used model in the SIF research community, since it also includes full modules for calculating photosynthesis and

energy budget. It couples the leaf-level physiological module of Chl*a*F emission (Van der Tol et al., 2014), the leaf-level RTM Fluspect (Vilfan et al., 2016, 2018), and the canopy-level RTM SAIL (Verhoef, 1984, 1985), with subsequent updates to incorporate canopy vertical heterogeneity and to improve computation efficiency (Yang, Prikaziuk, et al., 2021). SCOPE has emerged as a standard tool (or a synthetic "virtual truth") for process interpretation (e.g., Verrelst et al., 2015; Yang, Prikaziuk, et al., 2021) and for benchmarking other models, including both large-scale Terrestrial Biosphere Models (TBMs)/ Land Surface Models (LSMs) (e.g., Li et al., 2022) and small-scale complex 3D models (e.g., Zeng et al., 2020; Zhao et al., 2016). Furthermore, SCOPE has been taken as the standard paradigm for parameterizing leaf-level Chl*a*F emission and predominantly adopted (with varying actual implementations) by researchers into TBMs/LSMs (Parazoo et al., 2019). The basic strategy of SCOPE's leaf-level Chl*a*F emission parameterization (Fig. S1) is to 1) compute k_N (the rate constant of NPQ) as an empirical function of the degree of light saturation (derived from the actual and potential ETR), which in turn 2) closes the system of equations (i.e., having the number of equations equal the number of unknowns) for calculating photochemistry, non-photochemical heat dissipation, and PSII Chl*a*F emission according to the principle of energy conservation (i.e., Φ_{FII}, q_{LII}, NPQ form a closed equation for PSII, and knowing any two of them is sufficient to resolving the third, assuming Φ_{PSIIm} and k_{DF} are constants). This strategy, denoted as FvCB+ k_N, has to compute photosynthesis and actual ETR first, from FvCB, prior to derivation of k_N,NPQ, and SIF. It is subject to uncertainties propagated from parameter uncertainties present in FvCB (Rogers et al., 2017; Walker et al., 2021) and the empirical NPQ model for computing k_N. Indeed, the wide discrepancy of simulated SIF across TBMs/LSMs and deviations from observed SIF may result at least partly from these uncertainties (Parazoo et al., 2020; Yang, van der Tol, et al., 2021), as each individual model has different actual implementation of FvCB and k_N formulations. Moreover, this approach essentially conflicts with the original intention of using SIF in a forward mode to curb uncertainties in current photosynthesis estimates from FvCB.

The level of detail of the canopy radiative transfer representation in RTM essentially determines the computational demand and applicable scales (Table 1). For regional to global applications, the 1D SCOPE model with multi-layer treatment is practically unmanageable due to computational demand. Currently, global TBMs/LSMs usually employ the "big-leaf" strategy to simplify the canopy RTM. In these models, the SIF anisotropy cannot be explicitly modeled (Li et al., 2022), but most often treated as an empirical scaling factor derived from SCOPE ensemble simulations. Both SCOPE and the 3D family of models are capable of simulating the anisotropy impact on $F_{\Omega\uparrow}$ by explicitly specifying the sun-canopy-sensor geometry. The major limitations of 3D models are the significant computational demands that prevent them from global simulations, as well as required input of leaf/canopy structure/functional information that are often challenging to obtain. Detailed description of the strengths and weaknesses of each model is summarized in Table 1.

578 **Table 1. Summary of existing process-based models that have SIF-simulating capability.**
579

Model	Leaf-level parameterization of Chl*a*F emission		Canopy RTM of SIF	Sun-canopy-sensor geometry	λ_F	Application	Pros	Cons	CE^	Ref
	Leaf RTM	***Biochemical***								
3D (horizontally) heterogeneous canopy - *small scale scenes*										
DART[#]	Fluspect	None	Explicit modeling based on 3D ray-tracing		Full spectra	• Natural landscapes • *DART only*: including urban landscapes	• Suitable for small scale scenes with fine complex composition and structure • *DART only*: Integration with Lidar	• Computationally still too demanding to be applied at large scale (>100m), but more efficient approaches may emerge. • Requiring accurate leaf/canopy structural/functional info as priori input, which are often challenging to obtain • No leaf-level Chl*a*F emission formulation included (except FLiES) • No vertical heterogeneity in vegetation structure • Not yet thoroughly validated with in-situ data		(Gastellu-Etchegorry et al., 2017)
FluorWPS	Fluspect	As a function of PAR[&]								(Zhao et al., 2016)
FluorFLIGHT[#]	Fluspect	None								(Hernández-Clemente et al. 2017)
FLiES	FluoMODLeaf	FvCB + k_N								(Sakai et al., 2020)

FluorRTER	Fluspect	None	Explicit modeling based on SRTE			• Computationally more efficient than the ray-tracing approach • Potential for large-scale applications			(Zeng et al., 2020)
1D (horizontally) homogeneous canopy - *point to landscape scale*									
SCOPE	Fluspect	FvCB + k_N	**• Explicit modeling based on SAIL 4-stream approach** **• Multi-layer canopy (nlayer = 10LAI)[$]**	**Full spectra**	**• Process interpretation** **• Benchmarking for both 3D and global TBMs/LSMs**	**• Computationally more efficient than 3D models** **• Vertical heterogeneity in biochemical and/or biophysical properties**	**• Not suitable for horizontally heterogeneous canopy, e.g., crops with row structure, forests with complex architecture** **• Requiring accurate site-specific leaf/canopy structural/functional info as priori input, which are often challenging to obtain** **• k_N formulation empirical and susceptible to uncertainties in FvCB** **• Impact of biotic stress not represented**		(Van der Tol et al., 2009, 2014; van der Tol et al., 2019; Yang et al., 2017; Yang, Prikaziuk, et al., 2021)
1D (horizontally) homogeneous canopy - *global scale TBMs or LSMs*									
BETHY + SCOPE	Fluspect	FvCB +*	• Multi-layer canopy (nlayer = 60)	• Not explicitly represented • Only output	• Single wavelength • A	• Global (forward) simulations of	• Computationally most efficient	• Uncertainties in model structure (formulations) and	(Koffi et al., 2015)

JSBACH	None	FvCB + q_{LII}	• Multi-layer canopy (nlayer = 3) • Assuming a constant exponential attenuation factor of Chl*a*F emission, calibrated to SCOPE simulations	nadir and/or hemispherically -integrated TOC SIF (calibrated to SCOPE ensemble simulations) • *BETHY only*: No info provided • *JSBACH only*: No SIF magnitude, as no wavelength separation	conversion factor calibrated to SCOPE ensemble simulations • *BETHY only*: No info provided on wavelength adjustment	SIF for comparison with in-situ and/or satellite SIF retrievals • Data assimilation by ingesting SIF measurements to constrain parameters and/or variables related to GPP simulations	for large-scale simulations • Vertical heterogeneity in biochemical/bio physical properties (for some models)	parameters of FvCB, k_N, SIF parameterizations for global PFTs • Simplified SIF leaf-to-canopy RTM formulations • Depend on external simulations of SCOPE for deriving simple conversion factors or parameterizations to account for escape probability at certain viewing angle(s) and specific wavelength		(Thum et al., 2017)
SiB*	None	FvCB +*	• One "big-leaf" model NOT separating sunlit and shaded portions • Assuming a factor accounting for leaf to canopy scaling calibrated to SCOPE simulations							(Haynes et al., 2020)
ORCHIDEE	None		• A simplified empirical model calibrated to SCOPE ensemble simulations							(Bacour et al., 2019)
BEPS	None		• Two "big-leaf" model accounting for sunlit and shaded portions • Exponential							(Cui et al., 2020; Qiu et al.,

		attenuation factor of Chl*a*F emission as a function of LAI and clumping index • Scattering factor of Chl*a*F emission as a function of LAI			2019)
CLM*	None	• Two "big-leaf" model accounting for sunlit and shaded portions • CLM4: Assuming a factor accounting for leaf to canopy scaling calibrated to SCOPE simulations • CLM5: Separate calculation of canopy-level escape probability for sunlit and shaded portions according to Zeng et al. (2019)	• Empirically represented • Only output nadir and/or hemispherically -integrated TOC SIF		(Lee et al., 2015; Raczka et al., 2019; Li et al., 2022)

[&]Based on Rosema et al. (1998)

[#]RAdiation transfer Model Intercomparison (RAMI) participating model

*Subjective to version differences and/or formulation variants

^CE denotes computational efficiency; models are broadly sorted in increasing order of CE, color-coded in a warm (low CE) to cold

(high CE) spectrum.
[$]nlayer denotes number of canopy layers

3. The inference question: What aspects of terrestrial ecosystem structure, function, and service can be reliably inferred from remotely sensed SIF and how?

The relevance of SIF for inferring photosynthesis and the related ecosystem structural and functional information rests on the fact that Chl*a*F emission is directly coupled to the actual linear ETR from PSII to PSI (Gu et al., 2019). However, the canopy-leaving $F_{\uparrow}(\lambda_F)$ (or more broadly $F_{\boldsymbol{\Omega}\uparrow}(\lambda_F)$) needs to be converted to $F_{eT}(\lambda_F)$, prior to any meaningful inference of ecosystem structure or function. In the following, we first summarize current approaches that infer $F_{eT}(\lambda_F)$ from $F_{\uparrow}(\lambda_F)$ or $F_{\boldsymbol{\Omega}\uparrow}(\lambda_F)$ (3.1), and then present the full equations to estimate the actual ETR and GPP utilizing Chl*a*F emission as input (3.2). Finally, we develop a "toy" model as an analytical framework (3.3), which not only offers direct mechanistic insights on interpreting the relationship between $F_{\uparrow}(\lambda_F)$ and GPP at varying spatiotemporal scales or under different environmental conditions, but also enables a practical solution to compute regional/global GPP by taking remotely-sensed $F_{\uparrow}(\lambda_F)$ as input. Note in this paper, $F_{\uparrow}(\lambda_F)$ and $F_{\boldsymbol{\Omega}\uparrow}$ denote canopy-leaving SIF at TOC, which are assumed to be identical to the at-sensor SIF signal, i.e., negligible atmospheric absorption/scattering from the atmospheric column between TOC and the observing instrument, which is a reasonable assumption for solar Fraunhofer-line based SIF retrievals (Chang et al., 2020; Frankenberg et al., 2012).

3.1 Inferring $F_{eT}(\lambda_F)$ from $F_{\uparrow}(\lambda_F)$ or $F_{\boldsymbol{\Omega}\uparrow}(\lambda_F)$

There are two common approaches to infer $F_{eT}(\lambda_F)$. The **first** attempts to estimate the fluorescence escape probability $f^{esc}(\lambda_F) = \frac{F_{\uparrow}(\lambda_F)}{F_{eT}(\lambda_F)}$ escaping out of TOC (viewed from nadir), from the measured TOC reflectance $R(\lambda_F)$. More commonly for spaceborne measurements, the directional TOC SIF radiance (and also the directional TOC reflectance) at sun-canopy-sensor geometry $\boldsymbol{\Omega}\uparrow$ is acquired, i.e., $F_{\boldsymbol{\Omega}\uparrow}$; therefore the fluorescence escape probability is $\boldsymbol{\Omega}\uparrow$-dependent, i.e., $f^{esc}_{\Omega\uparrow}(\lambda_F) = \frac{F_{\boldsymbol{\Omega}\uparrow}(\lambda_F)}{F_{eT}(\lambda_F)}$. The term 'escape probability' originated from recollision theory (Stenberg 2007; Knyazikhin et al., 2011), and appears to exhibit a red edge pattern very similar to reflectance (Fig. 3). Therefore, this approach takes advantage of the similarity of photon interception and scattering behaviors between Chl*a*F emission and excitation irradiance (i.e., for paths after first interaction with leaves and inducing Chl*a*F emission) within a canopy (Fig. 3; Yang and van der Tol 2018). As directional TOC reflectance is widely available, facilitating this type of approach is a practical way to approximate f^{esc} or $f^{esc}_{\Omega\uparrow}$.

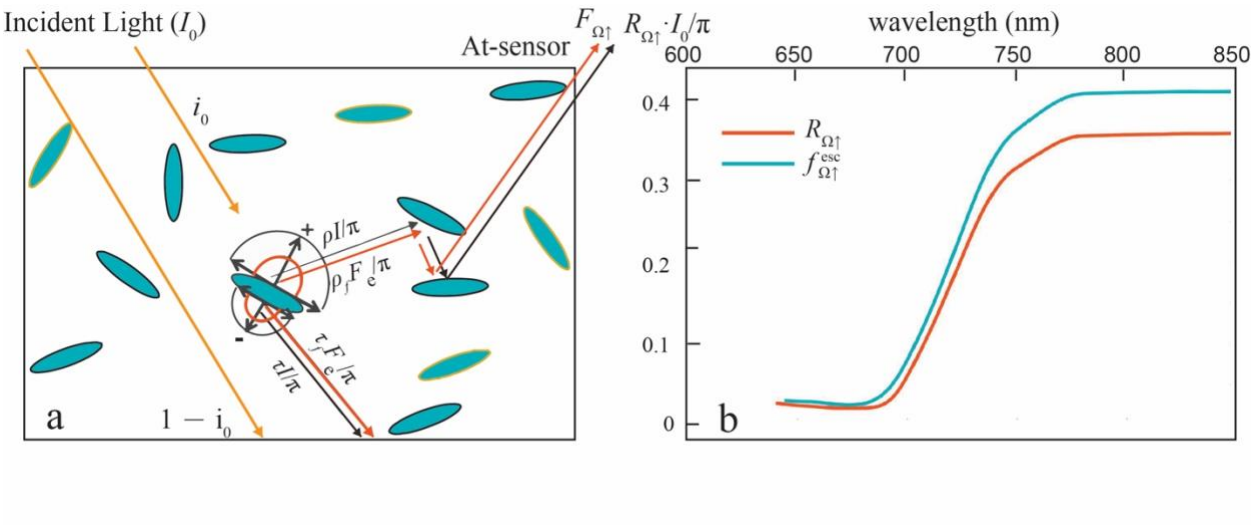

Fig. 3. Similarity between TOC fluorescence escape probability f^{esc} and reflectance. (a) A diagram illustrating the radiative transfer paths of incident solar radiation and SIF within a canopy, adopted from Yang & van der Tol (2018). Definition of symbols is in Table S1. Orange, black, and red arrows represent incoming solar radiation, reflected/transmitted solar radiation, reflected/transmitted fluorescence, respectively. ρ and τ denote leaf reflectance and transmittance respectively; ρ_f and τ_f denote the relative partitioning of Chl*a*F emission in the backward and forward direction respectively; i_0 is the canopy interceptance. (b) $f^{esc}_{\Omega\uparrow}$ and reflectance $R_{\Omega\uparrow}$ as a function of wavelength simulated with SCOPE2.1 for a homogeneous C3 crop canopy viewed from nadir (detailed model parameter setup in Table S2).

Yang & van der Tol (2018) demonstrated that irrespective of the complexity of radiative transfer, the relationship between $f^{esc}_{\Omega\uparrow}(\lambda_F)$ and $R_{\Omega\uparrow}(\lambda_F)$ of a canopy over a black soil (i.e., $r_s = 0$) can be expressed as:

$$f^{esc}_{\Omega\uparrow}(\lambda_F) = \frac{F_{\Omega\uparrow}(\lambda)}{F_{eT}(\lambda_F)} = \frac{R_{\Omega\uparrow}(\lambda_F)}{i_0 \cdot \omega(\lambda_F)} \quad (4)$$

here i_0 is the canopy interceptance (depending on canopy gap fraction, unitless), and ω is leaf scattering coefficients (i.e., the sum of leaf reflectance ρ and transmittance τ, unitless). Eq 4 indicates that canopy reflectance $R_{\Omega\uparrow}(\lambda_F)$ can serve as a practical solution to 'correct' $F_{\Omega\uparrow}(\lambda_F)$ for structure related effects that may otherwise overshadow those of quenching mechanisms of Chl*a*F emission. Eq 4 is the theoretical foundation for following derivations and implementations of varying forms, i.e., Eqs 5a-h summarized in Table 2. However, there are two caveats in Eq 4. First, i_0 and ω may not be accurately known as *a priori*; second, r_s is assumed as zero, which in reality may not be the case and can contribute to $R_{\Omega\uparrow}(\lambda_F)$ but not to Chl*a*F emission.

To address the first caveat, Yang et al. (2020) developed the Fluorescence Correction Vegetation Index (FCVI) (Eq 5b), the product of the fraction of absorbed photosynthetically active radiation $fPAR$ and $f^{esc}_{\Omega\uparrow}(\lambda_F)$, based on the radiative transfer theory. Here $R_{\Omega\uparrow}(vis)$ is the broadband visible directional reflectance over the PAR spectral range, and $R_{\Omega\uparrow}(NIR)$ is directional reflectance over the range of the NIR plateau (~750-900nm). FVCI quantifies the

combined effect of PAR absorption and SIF scattering, therefore accounting for the aggregated effect of leaf/canopy structure on SIF.

To address the second caveat, Zeng et al. (2019) proposed to use NDVI to differentiate $R_{\mathbf{\Omega}\uparrow}(NIR)$ of pure vegetation from soil, which does not contribute to Chl*a*F emission but impacts $R_{\mathbf{\Omega}\uparrow}(NIR)$, i.e., Eq 5f.

Note Eqs 4-5 are only valid when the sun-canopy-sensor geometries $\mathbf{\Omega}\uparrow$ are identical between far-red SIF and reflectance (i.e., measured at the same time from the same platform in practice). Furthermore, Eq 4 (and therefore Eqs 5a-d, f-g) is valid only for far-red SIF but not for red SIF, likely due to the asymmetry in the relative partitioning of scattering over two sides of a leaf (i.e., ρ vs τ) between incident solar radiation and Chl*a*F emission in the red region (Yang & van der Tol, 2018) and the significantly more re-absorption of Chl*a*F emission at red within a canopy. To remedy this issue, Liu et al. (2020) extends the $f_{\Omega\uparrow}^{esc}$ formulation to red SIF (Eq. 5e) using empirical approximation of $NDVI^2$ to mitigate soil contamination. Strictly speaking, $R_{\mathbf{\Omega}\uparrow}$ and $F_{\mathbf{\Omega}\uparrow}$ should be at the same wavelength λ_F, which in practice, are unfortunately not available if they are from different spaceborne instruments. Therefore, there is often a spectral mismatch between the far-red SIF and reflectance at NIR (e.g., Zeng et al., 2019). Other variants of $f_{\Omega\uparrow}^{esc}(\lambda_F)$ formulations and their corresponding caveats are summarized in Table 2.

Table 2. Summary of approaches developed to estimate $f_{\Omega\uparrow}^{esc}$ and concurrently to correct the BRDF (Bidirectional Reflectance Distribution Function) effect of $F_{\Omega\uparrow}$.

Approach	λ_F	Pros	Cons	Ref	SIF data	Reflectance data
Simple index based on reflectance and spectral invariant theory (analytical solution)						
$f_{\Omega\uparrow}^{esc}(\lambda_F) = \frac{R_{\Omega\uparrow}(\lambda_F)}{i_0 \cdot \omega(\lambda_F)}$ (4)	**far-red**	**C1; D1**	**T1, T2, T3; P1, P2, P3**	**Yang and van der Tol, 2018**	Synthetic	Synthetic
$f_{\Omega\uparrow}^{esc}(fr) = \frac{R_{\Omega\uparrow}(NIR)}{i_0 \cdot \omega(NIR)}$ (5a)	far-red	C1; D3, D4, D5; Mitigating T1, P1, P2	T2, T3; P3; S8	Zhang et al., 2019	TROPOMI	TROPOMI
$FCVI_{\Omega\uparrow}(fr) = fPAR \cdot f_{\Omega\uparrow}^{esc}(fr) = R_{\Omega\uparrow}(NIR) - R_{\Omega\uparrow}(\bar{vis})$ (5b)	far-red	C1; D1, D2, D4	T1, T2, T3; P3; S1, S3	Yang et al. 2020	*In-situ*	*In-situ*
$f_{\Omega\uparrow}^{esc}(fr) = \frac{BRF_{\Omega\uparrow}(NIR) \cdot NDVI}{i_0 \cdot \omega(NIR)}$ (5c)	far-red	D1, D2, D3, D4, D5; Mitigating T1, P1, P2	T1, T2, T3; P3; S2	Zhang et al., 2020	*In-situ*; OCO-2	*In-situ*; OCO-2
$f_{\Omega\uparrow}^{esc}(fr) = \frac{BRF_{\Omega\uparrow}(NIR) \cdot NDVI}{fPAR}$ (5d)	far-red	D1, D2, D4, D5; Mitigating T1, P1, P2	T1, T2, T3; P3; S1, S2	Liu et al.2020	*In-situ*	*In-situ*
$f_{\Omega\uparrow}^{esc}(r) = \frac{BRF_{\Omega\uparrow}(r) \cdot NDVI^2}{fPAR}$ (5e)	red	D1, D2, D4, D5; Mitigating T1, P1, P2	T2, T3; P3; S1, S2, S6	Liu et al., 2020	*In-situ*	*In-situ*

$f_{\Omega\uparrow}^{esc}(fr) = \frac{R_{\Omega\uparrow}(NIR) \cdot NDVI}{fPAR} = \frac{NIRv_{\Omega\uparrow}}{fPAR}$ (5f)	far-red	D1, D2, D4, D5; Mitigating T1	T2, T3; P1, P2, P3; S1, S2	Zeng et al., 2019	Synthetic; TROPOMI	Synthetic; MODIS
$F_{\Omega1}(fr) = F_{\Omega2}(fr) \cdot \frac{NIRv_{\Omega2}}{NIRv_{\Omega1}}$ (5g)	far-red	D2, D4, D5; Mitigating P1	T2, T3; P1, P2, P3; S2, S3, S4, S5	Hao, Asrar, et al.2021; Hao, Zeng, et al., 2021; Hao et al., 2022	*In-situ*; OCO-2; TROPOMI	*In-situ*; MODIS
$F_{\Omega1}(r) = F_{\Omega2}(r) \cdot \frac{R_{\Omega2}(r)}{R_{\Omega1}(r)}$ (5h)	red	D2, D4, D5; Mitigating P1	T2, T3; P1, P2, P3; S2, S3, S4, S5, S6	Hao, Zeng, et al., 2021; Hao et al., 2022	*In-situ*	*In-situ*
Kernel-driven approach	red, far-red	D4, D5	S3, S7	Hao, Zeng, et al., 2021; Hao et al., 2022	*In-situ*; TROPOMI	*In-situ*; MODIS
Explicit RTM model (numerical solution)						
A geometric-optical bidirectional model (simplified) accounting for separation of sunlit and shaded portions	far-red	• Theoretically rigorous derivation based on the geometric-optical bidirectional reflectance approach • Considering clumping index • Computationally affordable for global applications	• Assumption of constant sunlit vs shaded fractions • Theoretically valid for far-red only	He et al., 2017	GOME-2	NA
Data-driven approach						

Random forest with directional reflectances from red, red-edge, and far-red as input	red, far-red	• Computationally efficient • Training data from synthetic data generated from model simulations, relaxing the dependance on extensive observational data for training • Not requiring wavelength consistency between reflectance and SIF	• The global scalability is limited, as the machine learning type approach is known for weak capability for extrapolation • Uncertainties in training data propagated from uncertainties in structural/parameter models that are used for generating synthetic data	Liu et al., 2018	*In-situ*; HyPlant	*In-situ*; HyPlant

Note: fr and r denote far-red and red fluorescence wavelengths respectively; $\bar{vis}$ means integrated over the PAR spectral range; BRF denotes bidirectional reflectance factor.

- **C1**: Theoretically rigorous derivation based on spectral invariant RTM theory
- **T1**: Theoretically valid for black soil background only
- **T2**: Theoretically valid for far-red only, as the required assumption of the same partitioning between transmittance (forward) vs reflectance (backward) of PAR and forward vs backward Chl*a*F emission only valid at far-red
- **T3**: Chl*a*F emission excited by scattered PAR omitted in the theoretical derivation
- **D1**: Computational simplicity and efficiency
- **D2**: Required input widely available from existing spaceborne measurements
- **D3**: Considering impact of clumping index on canopy interceptance
- **D4**: Applicable to ecosystems with moderate to dense vegetation coverage
- **D5**: Possibly applicable to ecosystems with sparse vegetation coverage
- **P1**: Requiring identical sun-canopy-sensor geometry between far-red SIF and reflectance, currently challenging to obtain from spaceborne measurements from different platform/instruments
- **P2**: Requiring identical wavelength between far-red SIF and reflectance, which can be challenging for spaceborne measurements from different platform/instruments
- **P3**: No direct measurements of interceptance, which requires approximation
- **S1**: Approximation of $fPAR_{chl}$ ($fPAR$ from chlorophyll only) as $fPAR$
- **S2**: NDVI taken as a proxy of pure vegetation signal, excluding the soil effect on NIR reflectance, while NDVI not a perfect measure for "pure" vegetation
- **S3**: No estimation of F_{eT}

- **S4**: Only view angle, not solar angle
- **S5**: Requiring kernel-based BRDF model
- **S6**: Theoretical derivation involving many empirical approximation
- **S7**: Requiring multi-angle SIF measurements
- **S8**: Spaceborne reflected radiance not atmospherically corrected, affecting BRF calculation

The **second** type of approach relies on RTMs (Table 1) to numerically solve F_{eT} (e.g., Celesti et al., 2018; Yang et al., 2019), often with reflectance spectra as input to anchor the leaf/canopy structural parameters/variables that are required to invert RTMs. This approach may be feasible at the field or landscape scale but can be computationally formidable at regional and global scales. The FluorRTER RTM, with promising computational efficiency, offers potential to correct $f_{\Omega\uparrow}^{esc}$ of 3D canopies for airborne and satellite retrievals.

Other approaches to estimate $f_{\Omega\uparrow}^{esc}$ include data-driven (Liu, Liu et al., 2018) and kernel-driven approaches, which can effectively normalize $F_{\Omega\uparrow}$ into hotspot or nadir viewing directions if multi-angular SIF measurements are available (Hao, Asrar, et al., 2021; Hao et al., 2022; Hao, Zeng, et al., 2021).

3.2 The full equation: Deriving the canopy-level ETR and GPP

The total Chl*a*F emission consists of contributions from both PSII and PSI. Since the PSII emission dominates, and it can be easily probed with PAM fluorometry, Gu et al. (2019) related linear ETR and GPP to the PSII component of the total Chl*a*F emission. Further, as photochemistry, non-photochemical heat dissipation, and PSII Chl*a*F emission form a closed system according to the principle of energy conservation, the relationship between the actual linear ETR (J_a, μmol m^{-2} leaf area s^{-1}) and the PSII Chl*a*F emission can be expressed in terms of either redox states of PSII (q_{LII}) or NPQ. Note J_a refers to the actual ETR instead of the potential ETR (J_p) commonly used in the FvCB photosynthesis model (Farquhar et al., 1980). We derive the canopy-level total actual ETR (denoted as J_{aT}, μmol m^{-2} ground area s^{-1}) based on q_{LII} (Gu et al., 2019; Eq 21 therein).

$$J_{aT} = \int_0^{LAI} J_a(L)dL = \frac{\Phi_{PSIIm}(1+k_{DF})}{1-\Phi_{PSIIm}} \int_0^{LAI} p(L)q_{LII}(L) \int_{\lambda_{Fmin}}^{\lambda_{Fmax}} \int_{\lambda_{Imin}}^{\lambda_F} \Phi_{FII}(L)s_{II}(\lambda_F)\beta(L,\lambda_I)\sigma(L,\lambda_I)I(L,\lambda_I)d\lambda_I d\lambda_F dL \quad (6)$$

Here λ_{Fmin} and λ_{Fmax} denote the minimum and maximum wavelengths of Chl*a*F emission.

Further, GPP can be calculated by assuming: (1) all electrons from PSII are consumed either in carboxylation (CO_2 assimilation) or oxygenation (photorespiration), and alternative electron sinks such as nitrate reduction and Mehler reaction are negligibly small (Alric & Johnson, 2017); and (2) the light-carbon reactions are in perfect balance (Gu et al., 2019; Han, Chang, et al., 2022). These two assumptions are fairly accurate under normal conditions but may be violated when plants are under stress (Tcherkez & Limami, 2019). For example, if drought and heat stresses force stomatal closure when sunlight intensity is still high, a proportion of the liner electrons may flow to oxygen to form reactive oxygen species, rather than to NADP+ for carbon assimilation, which may break these two assumptions. To calculate GPP, one must further decide whether the carboxylation is limited by the supply of reduced power NADPH or energy currency ATP. In typical applications of FvCB, NADPH is assumed to be limiting, which

is adopted here to calculate the GPP of a canopy (denoted as GPP_T, μmol CO_2 m^{-2} ground area s^{-1}):

$$GPP_T \begin{cases} = \int_0^{LAI} \frac{C_c(L)-\Gamma^*(L)}{4C_c(L)+8\Gamma^*(L)} J_a(L)dL \\ = \frac{\Phi_{PSIIm}(1+k_{DF})}{1-\Phi_{PSIIm}} \int_0^{LAI} \frac{C_c(L)-\Gamma^*(L)}{4C_c(L)+8\Gamma^*(L)} q_{LII}(L) \int_{\lambda_{Fmin}}^{\lambda_{Fmax}} \int_{\lambda_{Imin}}^{\lambda_F} \Phi_{FII}(L) s_{II}(\lambda_F) \beta(L,\lambda_I) \sigma(L,\lambda_I) I(L,\lambda_I) d\lambda_I d\lambda_F dL & \text{(C3) (a)} \\ \\ = \int_0^{LAI} \frac{1-x}{3} J_a(L)dL \\ = \frac{\Phi_{PSIIm}(1+k_{DF})}{1-\Phi_{PSIIm}} \frac{1-x}{3} \int_0^{LAI} q_{LII}(L) \int_{\lambda_{Fmin}}^{\lambda_{Fmax}} \int_{\lambda_{Imin}}^{\lambda_F} \Phi_{FII}(L) s_{II}(\lambda_F) \beta(L,\lambda_I) \sigma(L,\lambda_I) I(L,\lambda_I) d\lambda_I d\lambda_F dL & \text{(C4) (b)} \end{cases}$$

(7)

Here C_c (Pa) is the CO_2 partial pressure in the stroma of chloroplast, Γ^* (Pa) is the CO_2 compensation point in the absence of day respiration, and x (unitless) is the fraction of total electron transport of mesophyll and bundle sheath allocated to mesophyll (for C4 plants only). Eqs 6-7 are the full equations to derive canopy-level ETR and GPP from Chl*a*F emission. Here q_{LII} (or NPQ) must be modeled independently in order to close the system, which remains as a major theoretical gap in current literature (2.4 and 4.1).

3.3 A toy model: Analytical solutions of canopy-level ETR and GPP from $F_{\uparrow}(\lambda_F)$

Comparison of Eqs 6-7 with 1-3 reveals that it is not straightforward to directly apply either $F_{\uparrow}(\lambda_F)$ or $F_{\boldsymbol{\Omega}\uparrow}(\lambda_F)$ or even $F_{eT}(\lambda_F)$ to estimate J_{aT} or GPP_T, as Eqs 6-7 require information on vertical distribution of Chl*a*F emission that are determined by variations in canopy structure/functions (Fig. 2). Therefore it is not conducive to directly employ Eqs 6-7 to compute J_{aT} or GPP_T analytically. To enable an analytical solution, we develop a toy model by simplifying Eq 3. Note here we utilize $F_{\uparrow}(\lambda_F)$ for demonstration; a corresponding formulation based on $F_{\boldsymbol{\Omega}\uparrow}(\lambda_F)$ can be similarly derived (or converting $F_{\boldsymbol{\Omega}\uparrow}(\lambda_F)$ to $F_{\uparrow}(\lambda_F)$ as a prior step). The major assumption to facilitate this simplification is that attenuation of emitted SIF and incoming PAR inside a canopy can be characterized with Beer's law (a commonly used strategy in global TBMs/LSMs). The toy model reads below (detailed derivation and other assumptions involved are provided in SI-6-8):

$$F_{\uparrow}(\lambda_F) = \underbrace{\varepsilon_{\uparrow 0}(\lambda_F) \left\{ \frac{1-e^{-(k_{PAR}+k_{\lambda_F})LAI}}{(k_{PAR}+k_{\lambda_F})LAI} + \frac{\varepsilon_{\downarrow 0}(\lambda_F) r_s(\lambda_F) \left[e^{-2k_{\lambda_F}LAI} - e^{-(k_{PAR}+k_{\lambda_F})LAI}\right]}{(k_{PAR}-k_{\lambda_F})LAI} \right\}}_{\text{Structure}} \times \underbrace{\left[\bar{\Phi}_{FII} s_{II}(\lambda_F)\bar{\beta} + \bar{\Phi}_{FI} s_I(\lambda_F)(1-\bar{\beta})\right]}_{\text{Mean ChlaF yield}} \times \underbrace{\overbrace{\bar{\rho} LAI}^{\text{Pigment}} \times \bar{\sigma} PAR_0}_{\text{Light harvesting}}$$

(8)

$$J_{aT} = \underbrace{\frac{\left(\frac{k_{\lambda_F}}{k_{PAR}}+1\right)\left[1-e^{-(b+1)k_{PAR}LAI}\right]}{\varepsilon_{\uparrow 0}(\lambda_F)\left[1-e^{-(k_{\lambda_F}+k_{PAR})LAI}\right]}}_{\text{Structure}} \times \underbrace{\frac{\Phi_{PSIIm}(1+k_{DF})}{1-\Phi_{PSIIm}}}_{\text{Constant}} \times \underbrace{\frac{\overbrace{\frac{aPAR_0^b}{b+1}}^{\text{Redox state}}}{s_{II}(\lambda_F)+\zeta s_I(\lambda_F)\frac{1-\bar{\beta}}{\bar{\beta}}}}_{\text{ChlaF weighting factor}} \times F_{\uparrow}(\lambda_F) \quad (9)$$

$$GPP_T = \underbrace{\frac{\left(\frac{k_{\lambda_F}}{k_{PAR}}+1\right)\left[1-e^{-(b+1)k_{PAR}LAI}\right]}{\varepsilon_{\uparrow 0}(\lambda_F)\left[1-e^{-(k_{\lambda_F}+k_{PAR})LAI}\right]}}_{\text{Structure}} \times \underbrace{\frac{\Phi_{PSIIm}(1+k_{DF})}{1-\Phi_{PSIIm}}}_{\text{Constant}} \times \underbrace{\frac{\overbrace{\frac{aPAR_0^b}{b+1}}^{\text{Redox state}}}{s_{II}(\lambda_F)+\zeta s_I(\lambda_F)\frac{1-\bar{\beta}}{\bar{\beta}}}}_{\text{ChlaF weighting factor}} \times F_{\uparrow}(\lambda_F) \times \begin{cases} \frac{C_c-\Gamma^*}{4C_c+8\Gamma^*} & \text{(C3) (a)} \\ \frac{1-x}{3} & \text{(C4) (b)} \end{cases} \quad (10)$$

Here $\varepsilon_{\uparrow 0}$ and $\varepsilon_{\downarrow 0}$ denote the upward/downward escape probability of Chl*a*F emission for an infinitesimally thin leaf layer at TOC/BOC respectively; $a$and b are empirical parameters for calculating q_{LII} as a function of PAR; $\bar{\Phi}_{FII}$ and $\bar{\Phi}_{FI}$ denote the canopy-level fluorescence quantum yield of PSII and PSI respectively under steady state; $\bar{p}$ denotes the mean photosynthetic pigment content of the canopy; $\bar{\beta}$ and $\bar{\sigma}$ are the canopy-mean broadband β and σ (i.e., integrated over the PAR spectral range 400 to 700nm) respectively.

Eq 8 represents a minimalistic model at the canopy level, which reveals that $F_{\uparrow}(\lambda_F)$ is affected by three groups of factors: leaf/canopy structure, the quantum yield of Chl*a*F emission (averaged between PSII and PSI), and light harvesting. The light harvested is the product of $\bar{p}$, $\bar{\sigma}$, and incident light intensity at TOC, i.e., PAR_0. The impact of leaf/canopy functions on Chl*a*F emission is represented by their impact on the mean quantum yield of Chl*a*F emission of a canopy. The canopy structure factor accounts for variations in the spatial display of photosynthetic pigments (*e.g.*, leaf orientation, vertical layering, pigment packaging, canopy rugosity, or porosity, etc, Fig. 2) that affects the light extinction coefficients of both Chl*a*F emission (denoted as k_{λ_F}) and intercepted irradiance for excitation (denoted as k_{PAR}). This toy model illustrates the joint control of leaf/canopy structure and functions as well as light harvesting on $F_{\uparrow}(\lambda_F)$. For example, two canopies with the same $\bar{p}$ can differ in $F_{\uparrow}(\lambda_F)$ if they differ in canopy/leaf structure or the mean quantum yield of Chl*a*F emission. This toy model is applicable for guiding process diagnosis and interpretation or knowledge inference on what structural and functional information can be inferred from $F_{\uparrow}(\lambda_F)$ (Sun et al., 2023b). We note that Eq 8 can be applied to a leaf by setting $LAI = 1$ and $r_s = 0$ (derivation in SI-6). Eqs 8 and S25 show that, even with considerable simplifications, additional inputs or constraints are always needed to reduce the degree of freedom to infer any structural or functional information from the

observed $F_{\uparrow}(\lambda_F)$ at the canopy or even the leaf level. What additional inputs are available determine how $F_{\uparrow}(\lambda_F)$ should be used and the level of complexity of such usage.

Eqs 9-10 present the analytical solution of canopy-level ETR and GPP utilizing at-sensor $F_{\uparrow}(\lambda_F)$ as input, facilitating a forward calculation of these quantities that are not subject to existing uncertainties in the full FvCB model and/or k_N formulations (i.e., the NPQ-based strategy). Parameters in these equations can be estimated from vertically distributed measurements of light attenuation, leaf PAM fluorometry and gas exchange. Moreover, Eqs 9-10 breaks J_{aT} and GPP_T into components of structure, a Chl*a*F weighting factor, and CO_2 diffusion (e^- use efficiency, for C3 only). Note that the toy model explicitly models $\varepsilon_{\uparrow}$ assuming it complies with Beer's law, and therefore does not have to separately correct f^{esc} before-hand, such as in 3.1. The system of Eqs 8-10 directly reveals what variables/parameters impact SIF and its relationship with GPP, in a more explicit fashion than the conventional light use efficiency (LUE) model. These analytical equations (along with those in SI) can be used to guide interpretation of SIF-GPP relationships, applications of SIF to different sectors under climate change, and innovations in observational instrumentation/setup (details in the companion paper, Sun et al., 2023b).

On the other hand, Eq 10 also suggests modeling GPP from at-sensor SIF is complex. Although the community shares the hope of utilizing remotely-sensed SIF to radically reduce the long-standing uncertainty in GPP estimates, we must acknowledge (from Eq 10): 1) SIF is not GPP, and 2) SIF is not a panacea to fix all issues (e.g., LAI,V_{cmax}, etc) that remain major contributors to the uncertainty in GPP estimation. First, the whole SIF dynamics is nonlinear (Eqs 3, 6, 7) which includes convoluted multiplications, integration, etc; hence integrated information in SIF (the direct observable) does not equal the integrated information in GPP (our target variable). Second, SIF is influenced by many factors that are shared with GPP (i.e., LAI, leaf angle,V_{cmax}, environmental forcings), so it can to some extent integrate over the dynamic physiological complexities of photosynthesis, and may offer a shortcut to model GPP bypassing some of the uncertainties in individual factors (e.g., V_{cmax} disappears in Eq. 10, Han, Chang, et al., 2022). However, LAI and clumping effect are still required in modeling GPP even though their impact is already (partly) incorporated by $F_{\uparrow}(\lambda_F)$.

4. Innovations: What innovations are needed to realize the full potential of SIF remote sensing for real-world applications under climate change?

Moving forward, to jigsaw individual "puzzle" pieces (i.e., the six blind men and the elephant) into holistic and insightful mosaics (via synthesis and synergy) towards the ultimate goal of depicting a full picture of the elephant, innovations are required in both theory development and observing technology (Sun et al., 2023b). Innovations in these aspects should fill existing theoretical and data gaps that currently challenge applications (summarized in Fig. 4). Below we summarize existing theoretical gaps (4.1, Fig 4), followed with our insights on potential innovative solutions to address them (4.2-4.3) guided by the analytical framework developed

above. Data gaps and corresponding innovative solutions are discussed in the companion data-perspective paper (Sun et al., 2023b).

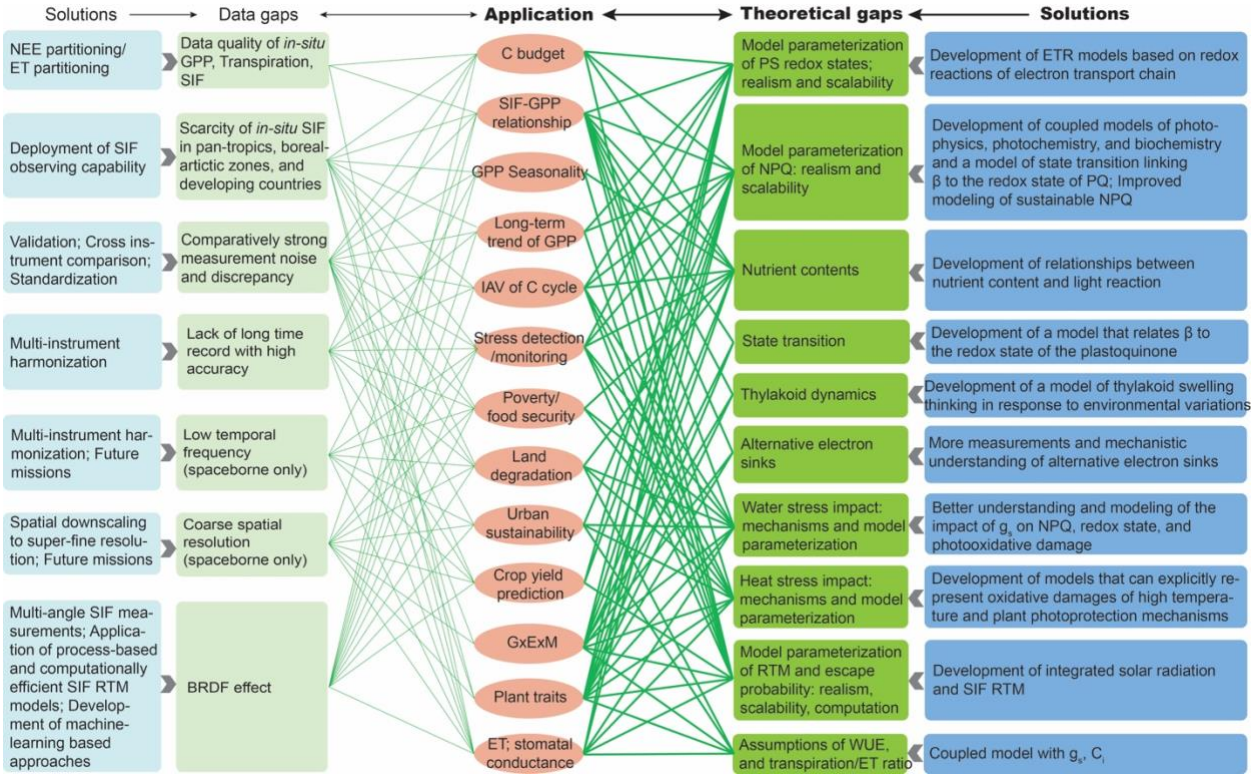

Fig. 4. Existing theoretical and data gaps through the lens of applications (Sun et al., 2023b), and potential solutions moving forward. This paper focuses on the theoretical side (the right columns highlighted in dark color) of this diagram. NEE: net ecosystem exchange.

4.1 Theoretical gaps

Our derivations of the equations governing SIF dynamics (Eq 3) and relationships with key ecophysiological variables (Eqs 6-10) (e.g., photosynthetic pigment, ETR, and GPP) point to where theoretical gaps exist and provide guidance on connecting individual dots into a complete picture across scales (Fig. 4). These gaps are not independent and filling them requires advances in broader areas of photosynthesis and ecological research.

The **redox states** of photosystems (i.e., q_{LII}, q_{LI}, q_7), as well regulated and unregulated **heat dissipations** (i.e., NPQ and $NPQ7$), play central roles in the dynamics of SIF and its relationships with pigment content, ETR, and GPP. It is difficult to utilize the full potential of SIF for ecophysiological applications without thoroughly understanding and modeling how redox state and NPQ processes affect the Chl*a*F emission (Eq 3). Either the redox states or NPQ must be known in order to utilize SIF to predict electron transport or GPP (Gu et al., 2019). The redox states and magnitudes of varoius heat dissipation pathways are an outcome of complex feedforward and feedback processes of photophysics, photochemistry, and biochemistry of photosynthesis. NPQ, q_{LII}, q_{LI}, and q_7 are sensitive to environmental stress and affected by

photodamage and photoinhibition, and change with phenology. The variations of NPQ and q_{LII} have often been studied by decomposing them into a sustainable (photo-inhibited) component and a reversible component (Porcar-Castell, 2011; Raczka et al., 2019; Tietz et al., 2017). The presence of photo-inhibited components increases NPQ, and decreases q_{LII} and Φ_{PSIIm}. Although the redox state and NPQ of PSII are routinely measured by PAM fluorometry and studied extensively, we currently still lack broadly applicable and mechanistically sound models to represent their dynamics in natural envionments. In particular, compared with our knowledge about the control of PSII redox states and NPQ, we currently know little about the control of PSI redox states and heat dissipation processes due to lack of measurements.

Nutrient content: Typically, the impact of nutrient contents on photosynthesis is investigated in terms of their relationship with photosynthetic capacity parameters such as the maximal carboxylation rate V_{cmax} and maximal potential electron transport rate J_{max}. For the applications of SIF, it is important to understand the mechanistic basis of the impact of nutrient availability on these photosynthetic capacity parameters. This is particularly important for J_{max} because electron transport (photochemistry) directly competes with SIF emission for energy partitioning. While the mechanism for the dependence of V_{cmax} on nutrient content is fairly well understood (e.g., Rubisco abundance depends on leaf nitrogen content LNC), how nutrient content mechanistically affects J_{max} is not clear, even though J_{max} and V_{cmax} exhibits empirical linear relationships (Wullschleger, S. D. 1993; Kattge and Knorr 2007). The "coordination theory" hypothesizes that plants can optimize LNC to balance Rubisco- and RuBP regeneration-limited carboxylation rates (Chen et al., 1993; Wang, Prentice, Keenan, et al., 2017), alluding the linkage between LNC and J_{max}. From the light reaction side, It has been reported that under the same environmental conditions, leaves with different nutrient contents may have different NPQ (Cheng, 2003) and q_{LII}. Also, foliar chlorophyll content depends on nutrient contents (Croft et al., 2017). It is likely that the foliar abundances of PSII and PSI and the stoichiometry between them also depend on nutrient availability; however, studies addressing this are rare.

State transition refers to the migration of mobile light-harvesting complexes II (LHCIIs) and thus the redistribution/rebalancing of energy absorption and excitation between PSII and PSI (for a review, see Minagawa (2011)). This process results in a dynamic adjustment of β. The energy balance between PSII and PSI is essential for the photosynthetic machinery to operate safely in fluctuating environments because these two types of photosystems are connected in series and the energy level of electrons transferred from PSII to PSI needs to be elevated by photons absorbed by the light harvesting complex of PSI. Thus, any imbalance between them can disrupt electron flow from PSII to PSI and to the eventual electron acceptor NADP+. When light regimes favor PSI, mobile LHCIIs in their de-phosphorylated form are attached to PSII, thus boosting its light harvesting and excitation. This condition is known as State 1. When light regimes change such that PSII is favored, mobile LHCIIs are phosphorylated and move to PSI to increase its absorption cross section, leading to State 2 of the photosystems. The energy imbalance between PSII and PSI and thus the need for state transition are sensed by the redox state of the pool of free plastoquinone (PQ) molecules which transport electrons within the

thylakoid membranes from PSII to Cyt. Currently we lack a quantitative model to predict state transition, and β is often assumed to be 0.5. But a change in the value of β will lead to a proportional change in Chl*a*F emission from PSII (Eqs 3 and 8), other conditions being equal. As a result, a dynamic β significantly impacts the response of Chl*a*F emission to variations in environmental conditions because of the change in energy allocation between PSII and PSI. Chl*a*F emission is believed to be dominated by PSII because PSI is photochemically more efficient than PSII (Hogewoning et al., 2012; Lazár, 2013). Thus, a change in PSII Chl*a*F emission cannot be compensated for by change in PSI Chl*a*F emission when β varies. Although state transition is often studied at short time scales (seconds to hours, Minagawa 2011), conceivably β could vary with canopy depth, phenology, species, and prevailing climate conditions (e.g. Porcar-Castell et al. 2014) which could affect the ratio of cyclic to linear electron transport required to support the Calvin-Benson Cycle, resulting in the need to rebalance the energy harvesting by the two photosystems. However, this remains uncharted and would deserve future attention.

Although it is a reasonable assumption that **PSI** plays a minor role in Chl*a*F emission when the overall energy level is considered, it is not clear whether this assumption is also valid over wavelengths at which SIF is retrieved from existing instruments. This issue is equivalent to asking whether any difference in the PSII and PSI spectral shape functions (s_{II} and s_I) is sufficiently small such that PSII Chl*a*F emission dominates at every wavelength. SIF cannot be observed in broadbands and has to be observed at Fraunhofer lines, O_2-A or -B bands. There is no *a priori* knowledge or observations to indicate how similar or different s_{II} and s_I are. Further studies on this issue either with theoretical analyses or observations are needed. If it turns out that PSI contribution cannot be ignored, then measurements and better understanding in the dynamics of q_{LI} and q_7 will be needed.

The **ultrastructure of thylakoids** is not static and has been observed to swell in the light and shrink in the dark (Li et al., 2020). The ultrastructural dynamics of thylakoids can regulate a number of processes that control photosynthetic ETR, including macromolecular blocking/collision probability, direct diffusional pathlength, Cyt duty division (Johnson and Berry 2021), luminal pH via osmotic water fluxes, and separation of pH dynamics between granal and lamellar lumens in response to environmental variations. Gu et al. (2022) discussed these impacts in detail. As photosynthetic ETR is directly coupled to Chl*a*F emission, the thylakoid ultrastructural dynamics induced by changes in environmental conditions can feedback to SIF dynamics (Eqs 6 and 9). Furthermore, pigments are located in the thylakoid membranes. As the thylakoid swells and shrinks, the pigment packing on the membranes will shift, affecting σ and thus photon interception and absorption and excitation energy transfer. Currently there is little knowledge regarding potential impacts of thylakoid ultrastructural dynamics on Chl*a*F emission.

Alternative electron sinks: ETR from PSII to PSI, which can be inferred from the Chl*a*F emission, supports not only photosynthesis but also other stromal metabolisms such as nitrate reduction, photoreduction of oxygen, and emission of volatile organic compounds (VOC). As a

result, ETR that supports photosynthesis is smaller than the rate that can be inferred from Chl*a*F emission and SIF measurements (Von Caemmerer, 2000). Alternative electron sinks serve as photoprotective mechanisms when plants are under stress and the energy harvested by photosystems exceeds the need of carboxylation and oxygenation. Thus alternative electron sinks can be strong under stressful environmental conditions (Alric & Johnson, 2017). The presence of alternative electron sinks is likely a key physiological mechanism affecting the SIF dynamics and the decoupling of SIF and GPP (Fig. 2 and Eqs3, 6-10), which remains uncharted and warrants future research.

Mechanisms and model parameterization of water and heat stress. One major knowledge gap is to pin down the exact mechanisms (e.g., leaf expansion/fall, heat dissipation, stomatal closure, hydraulic failure, carbon starvation) that plants use to respond and/or adapt to stress at different timescales, and how these stresses influence Chl*a*F emission and the observed SIF signal $F_{\uparrow}(\lambda_F)$. Filling this knowledge gap is crucial to enable SIF applications for inferring plant traits, selecting stress-tolerant crop genotypes/phenotypes, precision agriculture management, as well as regional-scale monitoring and early warning capacity for stress and food insecurity, etc (Sun et al., 2023b). A barrier is that SIF itself and its coupling with GPP is affected by a myriad of interactive processes and environmental variations (the forward issue, Eq 3), and thus the observed SIF $F_{\uparrow}(\lambda_F)$ reflects their collective and interactive effects (the inference issue, Eqs 9-10). Additional complexity would arise if multiple stresses co-occur, e.g., heatwave and drought, insect outbreak accompanied with water/heat stress, or flooding followed with nitrogen leaching, etc. Under such scenarios, SIF may reveal their amplified or compensating effect, but SIF alone is insufficient to tease out individual contributions. Observational and modeling innovations are needed to tackle these challenges (Sun et al., 2023b).

Connection of SIF to stomatal conductance and transpiration. The apparent correlation between SIF and transpiration obtained so far, although promising, is sensitive to three assumptions: a) the ratio of transpiration (T) to total evapotranspiration (ET) approaches to unity (during the peak growing season without rain events) (Lu et al., 2018; Shan et al., 2019), b) stomata optimize their openness to balance carbon uptake and water loss (Shan et al., 2019; Zhou et al., 2022), and c) SIF is linearly related to GPP. However, the first assumption holds only for certain ecosystems with high LAI (e.g., crops, deciduous forests) but not others (e.g., Mediterranean ecosystems); the second could be a reasonable assumption but the exact conditions under which it holds require future investigations (Stoy et al., 2019). The third assumption can be violated at shorter timescales and/or under stress (thorough discussion in 3.3 and Sun et al., 2023b).

Estimation of SIF escape probability: The majority of SIF applications across all sectors so far (Sun et al., 2023b) do not effectively correct the escape probability SIF although a variety of

practical approaches have recently emerged (Table 2), confounding the validity of their findings and mechanistic understanding. Strictly speaking, f^{esc} or $f^{esc}_{\Omega\uparrow}$ can only be explicitly estimated with RTMs of SIF, ideally with the ray tracing approach that specifies the 3D structure of plant canopy. From RTM theory, we can explain the magnitude and directionality of the variations in SIF and $f^{esc}_{\Omega\uparrow}$ induced by vegetation structure (Joiner et al., 2020). However, the computational demand prevents its practical applications especially at the ecosystem scale and beyond. The recent theoretical development of reflectance based approaches appears promising to approximate $f^{esc}_{\Omega\uparrow}$; however, attempts to correct it across biomes and different scales are often inconclusive due to both noisy SIF data (Sun et al., 2023b) and various assumptions/limitations in the $f^{esc}_{\Omega\uparrow}$ formulations (P1-S8 in Table 2).

4.2 Theoretical innovations at the leaf level: Coupling photophysics, photochemistry, and biochemistry

The key theoretical gaps identified above call for corresponding theoretical innovations in solutions (Fig. 5). These gaps are not independent, and filling them requires system thinking at the level of molecular mechanisms. To better understand how innovative solutions may be developed, we adopt the three stages of reactions of photosynthesis: photophysical reactions, photochemical reactions, and biochemical reactions. The necessity of dividing the light reactions into the photophysical and photochemical reactions is due to the fact that these two groups of reactions occur at different places with vastly different time scales and follow different laws.

Because the three stages are coupled, any equations that describe only one or two of the three reactions cannot be closed. For example, Eqs 1-3 and 6 are photophysical equations and can be applied only when additional information on variables such as NPQ and q_{LII} is supplied. Eq 7 attempts to couple photophysics and photochemistry to model GPP, which also requires additional modeling of NPQ and q_{LII}. The widely used FvCB model mechanistically describes the biochemical reactions, and depends on an empirical equation relating potential electron transport rate J_P to light intensity to provide a closure for modeling photosynthesis.

The weakest link in our efforts to relate SIF to GPP is photochemical reactions along the electron transport chain. The photochemical reactions are the bridge between the photophysical and biochemical reactions. While the models of photophysical and biochemical reactions have been sufficiently developed for SIF applications (Farquhar et al., 1980; Gu et al., 2019, Eqs 1-3, and 6), the same cannot be said for the photochemical reactions. Gu et al. (2023) derived analytical steady-state equations governing the states and redox reactions of complexes and electron carriers along the photosynthetic electron transport chain between PSII and Cyt. The impact of thylakoid ultrastructural dynamics on electron transport is represented by a light-induced thylakoid swelling/shrinking function that is applied to the fraction of Cyt available for linear electron transport. These equations are universal to oxygenic photosynthetic pathways, and allow the redox conditions of the mobile plastoquinone pool and Cyt to be inferred with typical

fluorometry. There are three critical next steps that need to be taken. One is to apply a similar approach and derive governing equations for electron transport from Cyt to PSI to NADP+ (linear transport) or to the PQ pool (cyclic transport around PSI) (J. E. Johnson & Berry, 2021). The second is to develop a model that links the redox state of mobile plastoquinone (PQ) with state transition. The redox state of PQ, which is already modeled in Gu et al. (2023), triggers state transition (Minagawa, 2011), and therefore could serve as a reliable predictor of state transition. The third is to develop a mechanistic model that could predict the alternative electron sinks, particularly VOC emissions, based on environmental conditions. Once these critical steps have been accomplished, a complete photochemical model will be established, allowing a full coupling of photophysical, photochemical, and biochemical reactions to mechanistically study SIF-GPP relationships.

Nevertheless, these steps are not easy and completing them will require substantial research efforts at time scales ranging from seconds to seasonal. In particular, the coupling of photophysics, photochemistry, and biochemistry will need to be tested for a wide range of environmental conditions including water and heat stresses. Both redox reactions and diffusion of electron carriers in photochemistry and enzymatic reactions in biochemistry are sensitive to temperature. Although temperature response functions are available, these functions have been rarely tested under extreme conditions. Water stress affects g_s and CO_2 supply to Rubisco, which will lead to feedback effects on the photophysical and photochemical reactions. At the present, these feedbacks have not been understood. Furthermore, stresses may damage organs and tissues such as photosystems and thylakoid membranes which would cause state change in the photosynthetic machinery, which is hard to model.

In the interim, empirical models of key photophysical and photochemical variables based on intensive and extensive PAM fluorometry measurements can be applied as temporary solutions to satisfy the need for process-based guidance for analyzing the rapidly increasing amount of SIF data. For example, simple light response functions of NPQ (Serôdio & Lavaud, 2011) and q_{LII} (Han, Chang, et al., 2022) can be used to satisfy modeling needs at diurnal time scales. The empirical relationship between the photochemical yield of PSII and NPQ as developed in Van der Tol et al. (2014) may also serve as a partial closure solution at conditions when variations in q_{LII} are small. Alternatively, one could potentially use estimated NPQ as inputs. NPQ can be estimated by monitoring the photochemical reflectance index over short time scales (Garbulsky et al., 2011). Nevertheless it must be emphasized these temporary solutions do not have general applicability and their validity must be evaluated on a case by case basis.

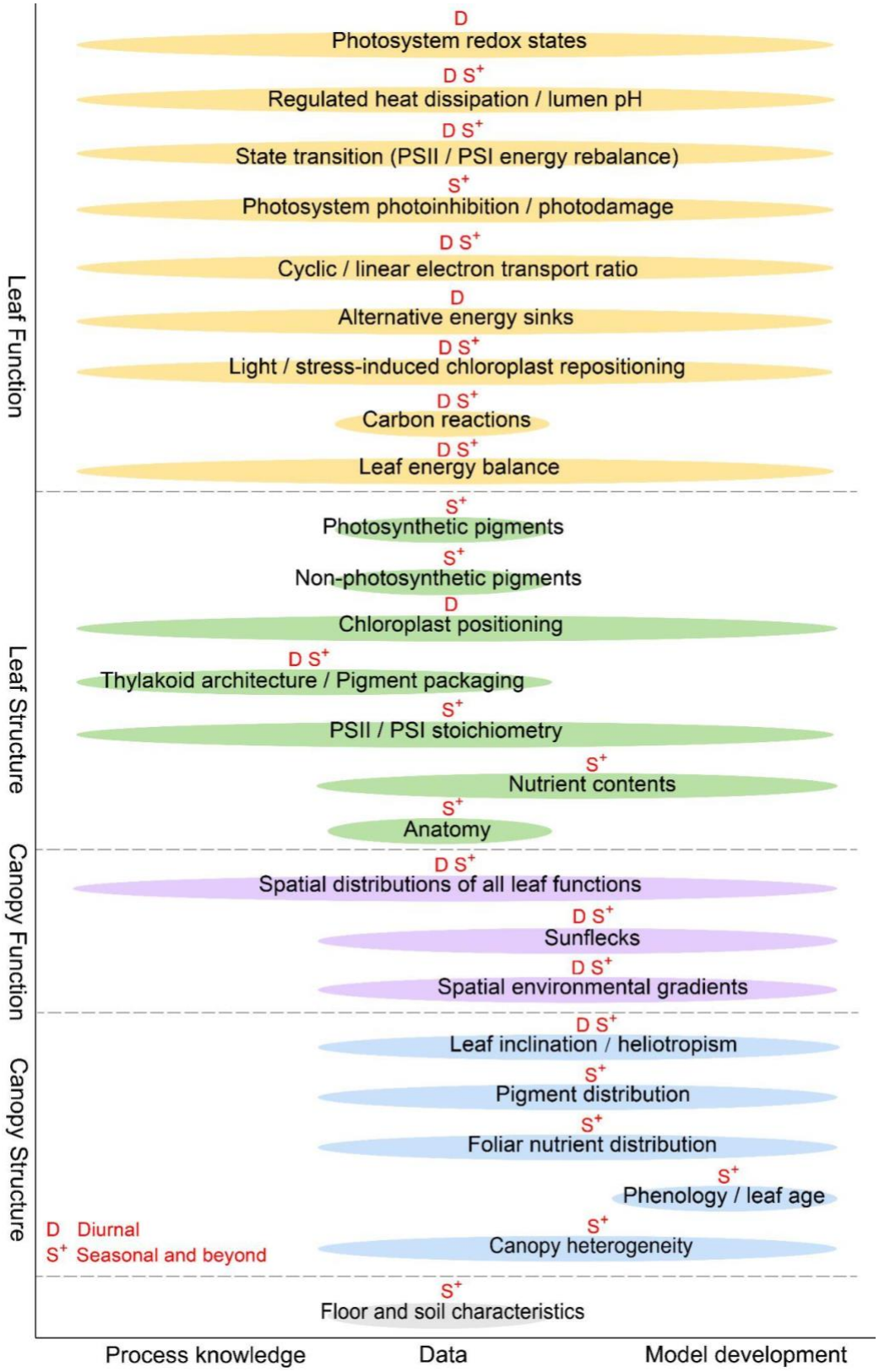

Fig. 5. Outlook for future SIF research efforts and priority. Research priority in mechanistic understanding, measurements, and model development respectively for each leaf/canopy

structure/function in Fig. 2 is mapped out. The letter D and S^+ denote diurnal scale and seasonal scale/beyond respectively, highlighting time scales each research effort should focus on.

4.3 Theoretical innovations at the canopy scale

Future research innovations at the canopy scale should focus on the following aspects.

Benchmarking RTM: Numerous leaf/canopy-level RTM with SIF capability have been developed at different levels of complexity, but their performance and applicability across biomes (with different leaf/canopy structures), landscape heterogeneities (with different composition/abundance of land covers), and biotic/abiotic stresses (with different symptomatic and asymptomatic spectral signatures) remains to be comprehensively evaluated. The RAdiation transfer Model Intercomparison (RAMI) protocol (Widlowski et al., 2015) well-established for surface reflectance can be adopted to benchmark SIF simulations. In particular, model validation with *in-situ* measurements of SIF (Parazoo et al., 2019; Yang et al., 2020), along with surface reflectance, e.g., SpecNet (Gamon et al., 2006), across diverse biomes and climate regimes is critical to ensure the realism of RTMs, despite the difficulty in concurrently obtaining latent quantities such as $F_{eT}(\lambda_F)$, and the actual leaf/soil optical properties. Moreover, the leaf/canopy RTM can be further integrated with atmospheric RTM to facilitate direct integration of at-sensor reflectance spectra (acquired by diverse platforms) (e.g., Yang et al., 2020). This can help address how the varying O_2-A depth between the direct and diffuse solar radiation impacts SIF retrieval from reflectance spectra, which remains one major challenge to disentangle solely from measurements.

Improving computational efficiency of RTM: The formidable computational demand of current RTMs (especially 3D) may be overcome with parsimonious surrogate models. For example, the FluorRTER RTM (Zeng et al., 2020) has similar performance to the full 3D ray-tracing FluorWPS, but is computationally much more affordable. Machine learning represents a promising pathway to effectively emulate complex physical processes with computational efficiency. Both approaches have the potential to make RTM inversions more accessible to users and more applicable at large spatial scales. For applications at global scales and/or spanning decades (e.g., constraining carbon budgets), a two-stream treatment of SIF RTM would be computationally more tangible (Li et al., 2022; Thum et al., 2017). In this case, an integrated solar radiation and SIF RTM should be developed based on the first principles of radiative transfer. From a physical point of view, the only difference between solar and SIF radiative transfer is that the source of solar radiation comes from the sun above the canopy top while the source of SIF is distributed within the canopy. Other than that, they follow the same physics. Furthermore, SIF radiative transfer is analogous to the longwave radiative transfer in plant canopies without the need to consider thermal emissions from sky; just like SIF, longwave radiation also has sources in plant canopies. Therefore, the highly efficient matrix approach for modeling longwave radiative transfer (Gu et al., 1999) can be modified to model SIF radiative

transfer in plant canopies. Either a two-stream or matrix-based SIF radiative transfer modeling approach, built upon basic physical principles, can be applied at regional to global scales.

Refinement of the toy model: The analytical framework developed here can be employed as an exploratory tool to facilitate process interpretation and diagnosis (Sun et al., 2023b), as it explicitly reveals the core and complex interacting mechanisms that are hidden in the light use efficiency models (Eqs 3, 6-8). Moreover, built upon theoretical understanding, the analytical solution has the potential to be applied universally across spatial and temporal scales towards various applications (Sun et al., 2023b). Nevertheless, in developing the toy model here, we have deliberately removed many details so that we can focus on core mechanisms; therefore it should be subject to rigorous test and refinement in the future due to various assumptions (detailed in SI). For example, the current form of leaf to canopy integration $\int_0^{LAI}$ is a highly conceptualized notation, and can take different forms with varying complexity in actual implementations. In the future, Eqs 8 and 10 can be expanded to separately model the sunlit and shaded components by explicitly accounting for the direct and diffuse solar radiation. This will inevitably introduce more complexities to model formulations. Moreover, Eqs 8-10 require additional information (beyond the integrated canopy functional/structural information carried in SIF), i.e., variables/parameters that are impacted by canopy structure (e.g., affecting solar and fluorescence attenuation), vertical distribution/variation of leaf functions (i.e., the redox states and/or NPQ) and pigment content/nutrient content (Fig. 5). Observational innovations are concurrently needed to facilitate model improvement in these aspects. On the other hand, Eq 10 can be used to diagnose the degree of linearity of SIF and GPP and contributing processes/parameters from the physiological and structural perspectives.

5. Conclusions

This review synthesizes theoretical understandings of photon harvesting, energy dissipation pathways and SIF radiative transfer in leaves and canopy to develop an analytical framework that 1) highlights the complex impacts of key leaf/canopy structure/function and their interactions on Chl*a*F emission and 2) guides the transformation of at-sensor SIF into meaningful information regarding photosynthetic electron transport and GPP. This framework enables identifying actionable solutions to tackle existing theoretical challenges and research priorities over the next 5-10 years. Key points this review aims to deliver are:

- **Harnessing theory and data**: Theories and data advancements should go hand-in-hand, in order to shift from correlational analyses to causal quantification and reasoning.
- **Appreciating the process complexity**: SIF is a single signal regulated by a myriad of complex biophysical, biochemical, and physiological processes in response to

environmental variations and anthropogenic perturbations. Inferring specific processes requires careful control of remaining interacting processes, with the aid of observation technology that can offer complementary information.

- **Versatile application potential of the toy model**. The toy model developed should be treated as an exploratory tool subject to rigorous test and refinement in the future due to various assumptions. Nevertheless, it conceptually represents a substantial improvement over light use efficiency models and can be employed at different spatial and temporal scales for process interpretation/diagnosis towards various applications (Sun et al., 2023b).

6. Acknowledgements

YS, JW, JL, ZL acknowledge support from NSF Macrosystem Biology (Award 1926488), NASA-CMS (80NSSC21K1058), NASA-FINESST (80NSSC20K1646), NASA MEaSures project, USDA-NIFA Hatch Fund (1014740), and the Cornell Initiative for Digital Agriculture Research Innovation Fund. CYC acknowledges support from USDA, Agricultural Research Service. JL acknowledges the Saltonstall Fellowship from the Soil and Crop Science Section at Cornell University. LH acknowledges support from NASA-IDS (80NSSC20K1263) and NASA-HAQAST (80NSSC21K0430). JJ is supported by NASA through the Arctic-Boreal Vulnerability Experiment (ABoVE) science team. LW acknowledges partial support from NSF Division of Earth Sciences (EAR-1554894). YS, JW, LH, and CBB also acknowledge support from USAID Feed the Future program (7200AA18CA00014). TSM acknowledges the Macrosystems Biology and NEON-Enabled Science program at NSF (award 1926090). ORNL is managed by UT-Battelle, LLC, for DOE under contract DE-AC05-00OR22725. We acknowledge Kathleen Kanaley for proofreading.

7. Reference

Aasen, Wittenberghe, V., Medina, Damm, Goulas, Wieneke, Hueni, Malenovský, Alonso, Pacheco-Labrador, Cendrero-Mateo, Tomelleri, Burkart, Cogliati, Rascher, & Arthur. (2019). Sun-Induced Chlorophyll Fluorescence II: Review of Passive Measurement Setups, Protocols, and Their Application at the Leaf to Canopy Level. Remote Sensing, 11(8), 927. https://doi.org/10.3390/rs11080927

Adams, W. W., & Demmig-Adams, B. (1992). Operation of the xanthophyll cycle in higher plants in response to diurnal changes in incident sunlight. Planta, 186(3), 390–398. https://doi.org/10.1007/BF00195320

Alric, J., & Johnson, X. (2017). Alternative electron transport pathways in photosynthesis: A confluence of regulation. Current Opinion in Plant Biology, 37, 78–86. https://doi.org/10.1016/j.pbi.2017.03.014

Anderson, J. M., Chow, W. S., & De Las Rivas, J. (2008). Dynamic flexibility in the structure and function of photosystem II in higher plant thylakoid membranes: The grana enigma. Photosynthesis Research, 98(1–3), 575–587. https://doi.org/10.1007/s11120-008-9381-3

Bacour, C., Maignan, F., MacBean, N., Porcar-Castell, A., Flexas, J., Frankenberg, C., Peylin, P., Chevallier, F., Vuichard, N., & Bastrikov, V. (2019). Improving Estimates of Gross Primary Productivity by Assimilating Solar-Induced Fluorescence Satellite Retrievals in a Terrestrial Biosphere Model Using a Process-Based SIF Model. Journal of Geophysical Research: Biogeosciences, 124(11), 3281–3306. https://doi.org/10.1029/2019JG005040

Barber, J., Alkin^, S. M., & Elfer, A. T. (1989). The origin of chlorophyll fluorescence In vivo and its quenching by the photosystem II reaction centre. Philosophical Transactions of the Royal Society of London. B, Biological Sciences, 323(1216), 227–239. https://doi.org/10.1098/rstb.1989.0006

Bittner, T., Irrgang, K. D., Renger, G., & Wasielewski, M. R. (1994). Ultrafast excitation energy transfer and exciton. Exciton annihilation processes in isolated light harvesting complexes of photosystem II (LHC II) from spinach. Journal of Physical Chemistry, 98(46), 11821–11826. https://doi.org/10.1021/j100097a004

Björkman, O., & Demmig, B. (1987). Photon yield of O2 evolution and chlorophyll fluorescence characteristics at 77 K among vascular plants of diverse origins. Planta. https://doi.org/10.1007/BF00402983

Browne, C., Matteson, D. S., McBride, L., Hu, L., Liu, Y., Sun, Y., Wen, J., & Barrett, C. B. (2021). Multivariate random forest prediction of poverty and malnutrition prevalence. PLOS ONE, 16(9), e0255519. https://doi.org/10.1371/JOURNAL.PONE.0255519

Caemmerer, S. von. (2000). Biochemical Models of Leaf Photosynthesis. In Techniques in Plant Sciences No 2.

Caffarri, S., Tibiletti, T., Jennings, R., & Santabarbara, S. (2014). A comparison between plant photosystem I and photosystem II architecture and functioning. Current Protein & Peptide Science, 15(4), 296–331. https://doi.org/10.2174/1389203715666140327102218

Cai, Y., Guan, K., Lobell, D., Potgieter, A. B., Wang, S., Peng, J., Xu, T., Asseng, S., Zhang, Y., You, L., & Peng, B. (2019). Integrating satellite and climate data to predict wheat yield in Australia using machine learning approaches. Agricultural and Forest Meteorology, 274, 144–159. https://doi.org/10.1016/j.agrformet.2019.03.010

Celesti, M., Tol, C. van der, Cogliati, S., Panigada, C., Yang, P., Pinto, F., Rascher, U., Miglietta, F., Colombo, R., & Rossini, M. (2018). Exploring the physiological information of Sun-induced chlorophyll fluorescence through radiative transfer model inversion. Remote Sensing of Environment, 215(May), 97–108. https://doi.org/10.1016/j.rse.2018.05.013

Cendrero-Mateo, Wieneke, Damm, Alonso, Pinto, Moreno, Guanter, Celesti, Rossini, Sabater, Cogliati, Julitta, Rascher, Goulas, Aasen, Pacheco-Labrador, & Arthur. (2019). Sun-Induced Chlorophyll Fluorescence III: Benchmarking Retrieval Methods and Sensor

Characteristics for Proximal Sensing. Remote Sensing, 11(8), 962. https://doi.org/10.3390/rs11080962

Chang, C. Y., Guanter, L., Frankenberg, C., Köhler, P., Gu, L., Magney, T. S., Grossmann, K., & Sun, Y. (2020). Systematic Assessment of Retrieval Methods for Canopy Far-Red Solar-Induced Chlorophyll Fluorescence Using High-Frequency Automated Field Spectroscopy. Journal of Geophysical Research: Biogeosciences, 125(7), e2019JG005533. https://doi.org/10.1029/2019JG005533

Chang, C. Y., Wen, J., Han, J., Kira, O., LeVonne, J., Melkonian, J., Riha, S. J., Skovira, J., Ng, S., Gu, L., Wood, J. D., Näthe, P., & Sun, Y. (2021). Unpacking the drivers of diurnal dynamics of sun-induced chlorophyll fluorescence (SIF): Canopy structure, plant physiology, instrument configuration and retrieval methods. Remote Sensing of Environment, 265, 112672. https://doi.org/10.1016/j.rse.2021.112672

Chen, J.-L., Reynolds, J. F., Harley, P. C., & Tenhunen, J. D. (1993). Coordination theory of leaf nitrogen distribution in a canopy. Oecologia, 93(1), 63–69. https://doi.org/10.1007/BF00321192

Cheng, L. (2003). Xanthophyll cycle pool size and composition in relation to the nitrogen content of apple leaves. Journal of Experimental Botany, 54(381), 385–393. https://doi.org/10.1093/JXB/ERG011

Chlorophyll a Fluorescence in Aquatic Sciences: Methods and Applications. (2010). In D. J. Suggett, O. Prášil, & M. A. Borowitzka (Eds.), Chlorophyll a Fluorescence in Aquatic Sciences: Methods and Applications. Springer Netherlands. https://doi.org/10.1007/978-90-481-9268-7

Coble, A. P., Fogel, M. L., & Parker, G. G. (2017). Canopy gradients in leaf functional traits for species that differ in growth strategies and shade tolerance. Tree Physiology, 37, 1415–1425. https://doi.org/10.1093/treephys/tpx048

Colombo, R., Celesti, M., Bianchi, R., Campbell, P. K. E., Cogliati, S., Cook, B. D., Corp, L. A., Damm, A., Domec, J. C., Guanter, L., Julitta, T., Middleton, E. M., Noormets, A., Panigada, C., Pinto, F., Rascher, U., Rossini, M., & Schickling, A. (2018). Variability of sun-induced chlorophyll fluorescence according to stand age-related processes in a managed loblolly pine forest. Global Change Biology, 24(7), 2980–2996. https://doi.org/10.1111/gcb.14097

Croft, H., Chen, J. M., Luo, X., Bartlett, P., Chen, B., & Staebler, R. M. (2017). Leaf chlorophyll content as a proxy for leaf photosynthetic capacity. Global Change Biology, 23(9), 3513–3524. https://doi.org/10.1111/GCB.13599

Cui, T., Sun, R., Xiao, Z., Liang, Z., & Wang, J. (2020). Simulating spatially distributed solar-induced chlorophyll fluorescence using a BEPS-SCOPE coupling framework. Agricultural and Forest Meteorology, 295, 108169. https://doi.org/10.1016/J.AGRFORMET.2020.108169

Damm, A., Guanter, L., Verhoef, W., Schläpfer, D., Garbari, S., & Schaepman, M. E. (2015). Impact of varying irradiance on vegetation indices and chlorophyll fluorescence derived

from spectroscopy data. Remote Sensing of Environment, 156, 202–215. https://doi.org/10.1016/j.rse.2014.09.031

Farquhar, G. D., Caemmerer, S., & Berry, J. A. (1980). A biochemical model of photosynthetic CO2 assimilation in leaves of C3 species. Planta, 149(1), 78-90–90.

Fisher, J. B., Huntzinger, D. N., Schwalm, C. R., & Sitch, S. (2014). Modeling the Terrestrial Biosphere. Annual Review of Environment and Resources, 39(1), 91–123. https://doi.org/10.1146/annurev-environ-012913-093456

Frankenberg, C., O'Dell, C., Guanter, L., & McDuffie, J. (2012). Remote sensing of near-infrared chlorophyll fluorescence from space in scattering atmospheres: Implications for its retrieval and interferences with atmospheric CO 2 retrievals. Atmospheric Measurement Techniques, 5(8), 2081–2094. https://doi.org/10.5194/amt-5-2081-2012

Gamon, J. A., Rahman, A. F., Dungan, J. L., Schildhauer, M., & Huemmrich, K. F. (2006). Spectral Network (SpecNet)-What is it and why do we need it? https://doi.org/10.1016/j.rse.2006.04.003

Garbulsky, M. F., Peñuelas, J., Gamon, J., Inoue, Y., & Filella, I. (2011). The photochemical reflectance index (PRI) and the remote sensing of leaf, canopy and ecosystem radiation use efficiencies: A review and meta-analysis. Remote Sensing of Environment, 115(2), 281–297. https://doi.org/10.1016/J.RSE.2010.08.023

Gastellu-Etchegorry, J. P., Lauret, N., Yin, T., Landier, L., Kallel, A., Malenovský, Z., Bitar, A. A., Aval, J., Benhmida, S., Qi, J., Medjdoub, G., Guilleux, J., Chavanon, E., Cook, B., Morton, D., Chrysoulakis, N., & Mitraka, Z. (2017). DART: Recent advances in remote sensing data modeling with atmosphere, polarization, and chlorophyll fluorescence. IEEE Journal of Selected Topics in Applied Earth Observations and Remote Sensing, 10(6), 2640–2649. https://doi.org/10.1109/JSTARS.2017.2685528

Gentine, P., Green, J. K., Guérin, M., Humphrey, V., Seneviratne, S. I., Zhang, Y., & Zhou, S. (2019). Coupling between the terrestrial carbon and water cycles—A review. Environmental Research Letters, 14(8), 083003. https://doi.org/10.1088/1748-9326/ab22d6

Govaerts, Y. M., Jacquemoud, S., Verstraete, M. M., & Ustin, S. L. (1996). Three-dimensional radiation transfer modeling in a dicotyledon leaf. Applied Optics, 35(33), 6585. https://doi.org/10.1364/AO.35.006585

Gu, L., Bernard, G., Han, J., Telesphore, M., Zhang, Y., Song, Y. C., & Sun, Y. (2023). An exploratory steady-state redox model of photosynthetic linear electron transport for use in complete modeling of photosynthesis for broad applications. Plant Cell and Environment. (accepted)

Gu, L., Grodzinski, B., Han, J., Marie, T., Zhang, Y.-J., Song, Y. C., & Sun, Y. (2022). Granal thylakoid structure and function: Explaining an enduring mystery of higher plants. New Phytologist, 236(2), 319–329. https://doi.org/10.1111/nph.18371

Gu, L., Han, J., Wood, J. D., Chang, C. Y. Y., & Sun, Y. (2019). Sun-induced Chl fluorescence and its importance for biophysical modeling of photosynthesis based on light reactions. New Phytologist, 223(3), 1179–1191. https://doi.org/10.1111/nph.15796

Gu, L., Shugart, H. H., Fuentes, J. D., Black, T. A., & Shewchuk, S. R. (1999). Micrometeorology, biophysical exchanges and NEE decomposition in a two-story boreal forest—Development and test of an integrated model. Agricultural and Forest Meteorology, 94(2), 123–148. https://doi.org/10.1016/S0168-1923(99)00006-4

Guan, K., Berry, J. A., Zhang, Y., Joiner, J., Guanter, L., Badgley, G., & Lobell, D. B. (2016). Improving the monitoring of crop productivity using spaceborne solar-induced fluorescence. Global Change Biology, 22(2), 716–726. https://doi.org/10.1111/gcb.13136

Guanter, L., Zhang, Y., Jung, M., Joiner, J., Voigt, M., Berry, J. a, Frankenberg, C., Huete, A. R., Zarco-Tejada, P., Lee, J.-E., Moran, M. S., Ponce-Campos, G., Beer, C., Camps-Valls, G., Buchmann, N., Gianelle, D., Klumpp, K., Cescatti, A., Baker, J. M., & Griffis, T. J. (2014). Global and time-resolved monitoring of crop photosynthesis with chlorophyll fluorescence. Proceedings of the National Academy of Sciences of the United States of America, 111(14), E1327-33. https://doi.org/10.1073/pnas.1320008111

Han, J., Chang, C. Y. Y., Gu, L., Zhang, Y., Meeker, E. W., Magney, T. S., Walker, A. P., Wen, J., Kira, O., McNaull, S., & Sun, Y. (2022). The physiological basis for estimating photosynthesis from Chla fluorescence. New Phytologist, 234(4), 1206–1219. https://doi.org/10.1111/NPH.18045

Han, J., Gu, L., Wen, J., & Sun, Y. (2022). Inference of photosynthetic capacity parameters from chlorophyll a fluorescence is affected by redox state of PSII reaction centers. Plant, Cell & Environment. https://doi.org/10.1111/PCE.14271

Hao, D., Asrar, G. R., Zeng, Y., Yang, X., Li, X., Xiao, J., Guan, K., Wen, J., Xiao, Q., Berry, J. A., & Chen, M. (2021). Potential of hotspot solar-induced chlorophyll fluorescence for better tracking terrestrial photosynthesis. Global Change Biology, 27(10), 2144–2158. https://doi.org/10.1111/GCB.15554

Hao, D., Zeng, Y., Qiu, H., Biriukova, K., Celesti, M., Migliavacca, M., Rossini, M., Asrar, G. R., & Chen, M. (2021). Practical approaches for normalizing directional solar-induced fluorescence to a standard viewing geometry. Remote Sensing of Environment, 255(December 2020), 112171. https://doi.org/10.1016/j.rse.2020.112171

Hao, D., Zeng, Y., Zhang, Z., Zhang, Y., Qiu, H., Biriukova, K., Celesti, M., Rossini, M., Zhu, P., Asrar, G. R., & Chen, M. (2022). Adjusting solar-induced fluorescence to nadir-viewing provides a better proxy for GPP. ISPRS Journal of Photogrammetry and Remote Sensing, 186, 157–169. https://doi.org/10.1016/J.ISPRSJPRS.2022.01.016

Hashimoto, H., Uragami, C., Yukihira, N., Gardiner, A. T., & Cogdell, R. J. (2018). Understanding/unravelling carotenoid excited singlet states. Journal of the Royal Society Interface, 15(141). https://doi.org/10.1098/RSIF.2018.0026

Haynes, K. D., Baker, I., & Denning, A. S. (n.d.). Simple Biosphere Model version 4.2 (SiB4) technical description. https://mountainscholar.org/handle/10217/200691

He, L., Chen, J. M., Liu, J., Mo, G., & Joiner, J. (2017). Angular normalization of GOME-2 Sun-induced chlorophyll fluorescence observation as a better proxy of vegetation productivity. Geophysical Research Letters, 44(11), 5691–5699. https://doi.org/10.1002/2017GL073708

Hernández-Clemente, R., North, P. R. J., Hornero, A., & Zarco-Tejada, P. J. (2017). Assessing the effects of forest health on sun-induced chlorophyll fluorescence using the FluorFLIGHT 3-D radiative transfer model to account for forest structure. Remote Sensing of Environment, 193, 165–179. https://doi.org/10.1016/j.rse.2017.02.012

Hertel, C., Leuchner, M., & Menzel, A. (2011). Vertical variability of spectral ratios in a mature mixed forest stand. Agricultural and Forest Meteorology, 151, 1096–1105. https://doi.org/10.1016/j.agrformet.2011.03.013

Hogewoning, S. W., Wientjes, E., Douwstra, P., Trouwborst, G., Ieperen, W. van, Croce, R., & Harbinson, J. (2012). Photosynthetic Quantum Yield Dynamics: From Photosystems to Leaves. The Plant Cell, 24(5), 1921–1935. https://doi.org/10.1105/tpc.112.097972

JOHNSON, G. N., YOUNG, A. J., SCHOLES, J. D., & HORTON, P. (1993). The dissipation of excess excitation energy in British plant species. Plant, Cell and Environment, 16(6), 673–679. https://doi.org/10.1111/j.1365-3040.1993.tb00485.x

Johnson, J. E., & Berry, J. A. (2021). The role of Cytochrome b 6f in the control of steady-state photosynthesis: A conceptual and quantitative model. In Photosynthesis Research (Vol. 148, Issue 3). Springer Netherlands. https://doi.org/10.1007/s11120-021-00840-4

Joiner, J., & Yoshida, Y. (2020). Satellite-based reflectances capture large fraction of variability in global gross primary production (GPP) at weekly time scales. Agricultural and Forest Meteorology, 291, 108092. https://doi.org/10.1016/j.agrformet.2020.108092

Joiner, J., Yoshida, Y., Köehler, P., Campbell, P., Frankenberg, C., van der Tol, C., Yang, P., Parazoo, N., Guanter, L., & Sun, Y. (2020). Systematic Orbital Geometry-Dependent Variations in Satellite Solar-Induced Fluorescence (SIF) Retrievals. Remote Sensing, 12(15), 2346. https://doi.org/10.3390/rs12152346

Kamen, M. D. (1963). Primary Processes in Photosynthesis (1st ed.).

Kattge, J., & Knorr, W. (2007). Temperature acclimation in a biochemical model of photosynthesis: A reanalysis of data from 36 species. Plant, Cell & Environment, 30(9), 1176–1190. https://doi.org/10.1111/j.1365-3040.2007.01690.x

Kautsky, H., & Hirsch, A. (1931). Neue Versuche zur Kohlens﷿ureassimilation. Die Naturwissenschaften, 19(48), 964–964. https://doi.org/10.1007/BF01516164

Knyazikhin, Y., Schull, M. A., Xu, L., Myneni, R. B., & Samanta, A. (2011). Canopy spectral invariants. Part 1: A new concept in remote sensing of vegetation. Journal of Quantitative Spectroscopy and Radiative Transfer, 112(4), 727–735. https://doi.org/10.1016/j.jqsrt.2010.06.014

Koffi, E. N., Rayner, P. J., Norton, A. J., Frankenberg, C., & Scholze, M. (2015). Investigating the usefulness of satellite-derived fluorescence data in inferring gross primary productivity within the carbon cycle data assimilation system. Biogeosciences, 12(13), 4067–4084. https://doi.org/10.5194/BG-12-4067-2015

Kramer, D. M., & Evans, J. R. (2011). The importance of energy balance in improving photosynthetic productivity. Plant Physiology, 155(1), 70–78. https://doi.org/10.1104/PP.110.166652

Kromdijk, J., Głowacka, K., Leonelli, L., Gabilly, S. T., Iwai, M., Niyogi, K. K., & Long, S. P. (2016). Improving photosynthesis and crop productivity by accelerating recovery from photoprotection. Science, 354(6314), 857–861. https://doi.org/10.1126/SCIENCE.AAI8878/SUPPL_FILE/KROMDIJK-SM.PDF

Laisk, A., Oja, V., Eichelmann, H., & Dall'Osto, L. (2014). Action spectra of photosystems II and i and quantum yield of photosynthesis in leaves in State 1. Biochimica et Biophysica Acta - Bioenergetics, 1837(2), 315–325. https://doi.org/10.1016/j.bbabio.2013.12.001

Latimer, P., Bannister, T. T., & Rabinowitch, E. (1956). Quantum Yields of Fluorescence of Plant Pigments. Science, 124(3222), 585–586. https://doi.org/10.1126/science.124.3222.585

Lazár, D. (2013). Simulations show that a small part of variable chlorophyll a fluorescence originates in photosystem I and contributes to overall fluorescence rise. Journal of Theoretical Biology, 335, 249–264. https://doi.org/10.1016/j.jtbi.2013.06.028

Lee, J.-E., Berry, J. A., Tol, C. van der, Yang, X., Guanter, L., Damm, A., Baker, I., & Frankenberg, C. (2015). Simulations of chlorophyll fluorescence incorporated into the Community Land Model version 4. Global Change Biology, 21(9), 3469–3477. https://doi.org/10.1111/gcb.12948

Li, M., Mukhopadhyay, R., Svoboda, V., Oung, H. M. O., Mullendore, D. L., & Kirchhoff, H. (2020). Measuring the dynamic response of the thylakoid architecture in plant leaves by electron microscopy. Plant Direct, 4(11). https://doi.org/10.1002/pld3.280

Li, R., Lombardozzi, D., Shi, M., Frankenberg, C., Parazoo, N. C., Köhler, P., Yi, K., Guan, K., & Yang, X. (2022). Representation of Leaf-to-Canopy Radiative Transfer Processes Improves Simulation of Far-Red Solar-Induced Chlorophyll Fluorescence in the Community Land Model Version 5. Journal of Advances in Modeling Earth Systems, 14(3), e2021MS002747. https://doi.org/10.1029/2021MS002747

Li, X., Xiao, J., He, B., Arain, M. A., Beringer, J., Desai, A. R., Emmel, C., Hollinger, D. Y., Krasnova, A., Mammarella, I., Noe, S. M., Ortiz, P. S., Rey-Sanchez, A. C., Rocha, A. V., & Varlagin, A. (2018). Solar-induced chlorophyll fluorescence is strongly correlated with terrestrial photosynthesis for a wide variety of biomes: First global analysis based on OCO-2 and flux tower observations. Global Change Biology, 24(9), 3990–4008. https://doi.org/10.1111/gcb.14297

Li, Y., He, N., Hou, J., Xu, L., Liu, C., Zhang, J., Wang, Q., Zhang, X., & Wu, X. (2018). Factors influencing leaf chlorophyll content in natural forests at the biome scale. Frontiers in Ecology and Evolution, 6(JUN), 64. https://doi.org/10.3389/FEVO.2018.00064/BIBTEX

Liu, X., & Liu, L. (2018). Influence of the canopy BRDF characteristics and illumination conditions on the retrieval of solar-induced chlorophyll fluorescence. International Journal of Remote Sensing, 39(6), 1782–1799. https://doi.org/10.1080/01431161.2017.1404165

Liu, X., Liu, L., Hu, J., Guo, J., & Du, S. (2020). Improving the potential of red SIF for estimating GPP by downscaling from the canopy level to the photosystem level.

Agricultural and Forest Meteorology, 281, 107846. https://doi.org/10.1016/J.AGRFORMET.2019.107846

Liu, Z., Ballantyne, A. P., Poulter, B., Anderegg, W. R. L., Li, W., Bastos, A., & Ciais, P. (2018). Precipitation thresholds regulate net carbon exchange at the continental scale. Nature Communications, 9(1), 1–10. https://doi.org/10.1038/s41467-018-05948-1

Lu, X., Liu, Z., An, S., Miralles, D. G., Maes, W., Liu, Y., & Tang, J. (2018). Potential of solar-induced chlorophyll fluorescence to estimate transpiration in a temperate forest. Agricultural and Forest Meteorology, 252(January), 75–87. https://doi.org/10.1016/j.agrformet.2018.01.017

Magney, T. S., Barnes, M. L., & Yang, X. (2020). On the Covariation of Chlorophyll Fluorescence and Photosynthesis Across Scales. Geophysical Research Letters, 47(23), e2020GL091098. https://doi.org/10.1029/2020GL091098

Magney, T. S., Bowling, D. R., Logan, B. A., Grossmann, K., Stutz, J., Blanken, P. D., Burns, S. P., Cheng, R., Garcia, M. A., Köhler, P., Lopez, S., Parazoo, N. C., Raczka, B., Schimel, D., & Frankenberg, C. (2019). Mechanistic evidence for tracking the seasonality of photosynthesis with solar-induced fluorescence. Proceedings of the National Academy of Sciences, 116(24), 11640–11645. https://doi.org/10.1073/pnas.1900278116

Malnoë, A. (2018). Photoinhibition or photoprotection of photosynthesis? Update on the (newly termed) sustained quenching component qH. Environmental and Experimental Botany, 154, 123–133. https://doi.org/10.1016/j.envexpbot.2018.05.005

Martini, D., Sakowska, K., Wohlfahrt, G., Pacheco-Labrador, J., Tol, C. van der, Porcar-Castell, A., Magney, T. S., Carrara, A., Colombo, R., El-Madany, T. S., Gonzalez-Cascon, R., Martín, M. P., Julitta, T., Moreno, G., Rascher, U., Reichstein, M., Rossini, M., & Migliavacca, M. (2022). Heatwave breaks down the linearity between sun-induced fluorescence and gross primary production. New Phytologist, 233(6), 2415–2428. https://doi.org/10.1111/NPH.17920

Miao, G., Guan, K., Yang, X., Bernacchi, C. J., Berry, J. A., DeLucia, E. H., Wu, J., Moore, C. E., Meacham, K., & Cai, Y. (2018). Sun-Induced Chlorophyll Fluorescence, Photosynthesis, and Light Use Efficiency of a Soybean Field from Seasonally Continuous Measurements. Journal of Geophysical Research: Biogeosciences, 123(2), 610–623.

Minagawa, J. (2011). State transitions—The molecular remodeling of photosynthetic supercomplexes that controls energy flow in the chloroplast. Biochimica et Biophysica Acta (BBA) - Bioenergetics, 1807(8), 897–905. https://doi.org/10.1016/j.bbabio.2010.11.005

Mohammed, G. H., Colombo, R., Middleton, E. M., Rascher, U., Tol, C. van der, Nedbal, L., Goulas, Y., Pérez-Priego, O., Damm, A., Meroni, M., Joiner, J., Cogliati, S., Verhoef, W., Malenovský, Z., Gastellu-Etchegorry, J. P., Miller, J. R., Guanter, L., Moreno, J., Moya, I., … Zarco-Tejada, P. J. (2019). Remote sensing of solar-induced chlorophyll fluorescence (SIF) in vegetation: 50 years of progress. Remote Sensing of Environment, 231(February), 111177. https://doi.org/10.1016/j.rse.2019.04.030

Mueller, N. D., Butler, E. E., Mckinnon, K. A., Rhines, A., Tingley, M., Holbrook, N. M., & Huybers, P. (2016). Cooling of US Midwest summer temperature extremes from cropland intensification. Nature Climate Change, 6(3), 317–322. https://doi.org/10.1038/nclimate2825

Pacheco-Labrador, Hueni, Mihai, Sakowska, Julitta, Kuusk, Sporea, Alonso, Burkart, Cendrero-Mateo, Aasen, Goulas, & Arthur, M. (2019). Sun-Induced Chlorophyll Fluorescence I: Instrumental Considerations for Proximal Spectroradiometers. Remote Sensing, 11(8), 960. https://doi.org/10.3390/rs11080960

Papageorgiou, G. C. & Govindjee. (2004). Chlorophyll a Fluorescence (G. C. Papageorgiou & Govindjee, Eds.; Vol. 19). Springer Netherlands. https://doi.org/10.1007/978-1-4020-3218-9

Parazoo, N. C., Frankenberg, C., Köhler, P., Joiner, J., Yoshida, Y., Magney, T., Sun, Y., & Yadav, V. (2019). Towards a Harmonized Long-Term Spaceborne Record of Far-Red Solar-Induced Fluorescence. Journal of Geophysical Research: Biogeosciences, 124(8), 2518–2539. https://doi.org/10.1029/2019JG005289

Parazoo, N. C., Magney, T., Norton, A., Raczka, B., Bacour, C., Maignan, F., Baker, I., Zhang, Y., Qiu, B., Shi, M., MacBean, N., Bowling, D. R., Burns, S. P., Blanken, P. D., Stutz, J., Grossmann, K., & Frankenberg, C. (2020). Wide discrepancies in the magnitude and direction of modeled solar-induced chlorophyll fluorescence in response to light conditions. Biogeosciences, 17(13), 3733–3755. https://doi.org/10.5194/BG-17-3733-2020

Pedrós, R., Goulas, Y., Jacquemoud, S., Louis, J., & Moya, I. (2010). FluorMODleaf: A new leaf fluorescence emission model based on the PROSPECT model. Remote Sensing of Environment, 114(1), 155–167. https://doi.org/10.1016/j.rse.2009.08.019

Peng, B., Guan, K., Zhou, W., Jiang, C., Frankenberg, C., Sun, Y., He, L., & Köhler, P. (2020). Assessing the benefit of satellite-based Solar-Induced Chlorophyll Fluorescence in crop yield prediction. International Journal of Applied Earth Observation and Geoinformation, 90, 102126. https://doi.org/10.1016/j.jag.2020.102126

Pierrat, Z., Magney, T., Parazoo, N. C., Grossmann, K., Bowling, D. R., Seibt, U., Johnson, B., Helgason, W., Barr, A., Bortnik, J., Norton, A., Maguire, A., Frankenberg, C., & Stutz, J. (2022). Diurnal and Seasonal Dynamics of Solar-Induced Chlorophyll Fluorescence, Vegetation Indices, and Gross Primary Productivity in the Boreal Forest. Journal of Geophysical Research: Biogeosciences, 127(2), e2021JG006588. https://doi.org/10.1029/2021JG006588

Porcar-Castell, A. (2011). A high-resolution portrait of the annual dynamics of photochemical and non-photochemical quenching in needles of Pinus sylvestris. Physiologia Plantarum. https://doi.org/10.1111/j.1399-3054.2011.01488.x

Porcar-Castell, A., Malenovský, Z., Magney, T., Van Wittenberghe, S., Fernández-Marín, B., Maignan, F., Zhang, Y., Maseyk, K., Atherton, J., Albert, L. P., Robson, T. M., Zhao, F., Garcia-Plazaola, J.-I., Ensminger, I., Rajewicz, P. A., Grebe, S., Tikkanen, M., Kellner, J. R., Ihalainen, J. A., … Logan, B. (2021). Chlorophyll a fluorescence illuminates a path

connecting plant molecular biology to Earth-system science. Nature Plants, 7(8), 998–1009. https://doi.org/10.1038/s41477-021-00980-4

Porcar-Castell, A., Tyystjärvi, E., Atherton, J., Tol, C. V. D., Flexas, J., Pfündel, E. E., Moreno, J., Frankenberg, C., & Berry, J. A. (2014). Linking chlorophyll a fluorescence to photosynthesis for remote sensing applications: Mechanisms and challenges. Journal of Experimental Botany, 65(15), 4065–4095. https://doi.org/10.1093/jxb/eru191

Qiu, B., Chen, J. M., Ju, W., Zhang, Q., & Zhang, Y. (2019). Simulating emission and scattering of solar-induced chlorophyll fluorescence at far-red band in global vegetation with different canopy structures. Remote Sensing of Environment, 233, 111373. https://doi.org/10.1016/J.RSE.2019.111373

Raczka, B., Porcar-Castell, A., Magney, T., Lee, J. E., Köhler, P., Frankenberg, C., Grossmann, K., Logan, B. A., Stutz, J., Blanken, P. D., Burns, S. P., Duarte, H., Yang, X., Lin, J. C., & Bowling, D. R. (2019). Sustained Nonphotochemical Quenching Shapes the Seasonal Pattern of Solar-Induced Fluorescence at a High-Elevation Evergreen Forest. Journal of Geophysical Research: Biogeosciences, 124(7), 2005–2020. https://doi.org/10.1029/2018JG004883

Rogers, A., Serbin, S. P., Ely, K. S., Sloan, V. L., & Wullschleger, S. D. (2017). Terrestrial biosphere models underestimate photosynthetic capacity and CO 2 assimilation in the Arctic. New Phytologist, 216(4), 1090–1103. https://doi.org/10.1111/nph.14740

Rosema, A., Snel, J. F. H., Zahn, H., Buurmeijer, W. F., & Hove, L. W. A. V. (1998). The relation between laser-induced chlorophyll fluorescence and photosynthesis. Remote Sensing of Environment, 65(2), 143–154. https://doi.org/10.1016/S0034-4257(98)00020-0

Ross, J. (1981). The radiation regime and architecture of plant stands. https://books.google.com/books?hl=en&lr=&id=w6SogqDOa54C&oi=fnd&pg=PP9&dq=Ross,+J.,+1981.+The+Radiation+Regime+and+Architecture+of+Plant+Stands.+Junk+Publishers,+The&ots=Z1b8CQ98AN&sig=5WZXz5JGyPtrYMqiSYKskVaDNWo

Ruban, A. V. (2016). Nonphotochemical Chlorophyll Fluorescence Quenching: Mechanism and Effectiveness in Protecting Plants from Photodamage. Plant Physiology, 170(4), 1903–1916. https://doi.org/10.1104/PP.15.01935

Sakai, Y., Kobayashi, H., & Kato, T. (2020). FLiES-SIF version 1.0: Three-dimensional radiative transfer model for estimating solar induced fluorescence. Geoscientific Model Development, 13(9), 4041–4066. https://doi.org/10.5194/GMD-13-4041-2020

Serôdio, J., & Lavaud, J. (2011). A model for describing the light response of the nonphotochemical quenching of chlorophyll fluorescence. Photosynthesis Research, 108(1), 61–76. https://doi.org/10.1007/s11120-011-9654-0

Shan, N., Ju, W., Migliavacca, M., Martini, D., Guanter, L., Chen, J., Goulas, Y., & Zhang, Y. (2019). Modeling canopy conductance and transpiration from solar-induced chlorophyll fluorescence. Agricultural and Forest Meteorology, 268, 189–201. https://doi.org/10.1016/j.agrformet.2019.01.031

Sloat, L. L., Lin, M., Butler, E. E., Johnson, D., Holbrook, N. M., Huybers, P. J., Lee, J. E., & Mueller, N. D. (2021). Evaluating the benefits of chlorophyll fluorescence for in-season crop productivity forecasting. Remote Sensing of Environment, 260, 112478. https://doi.org/10.1016/j.rse.2021.112478

Smith, W. K., Biederman, J. A., Scott, R. L., Moore, D. J. P., He, M., Kimball, J. S., Yan, D., Hudson, A., Barnes, M. L., MacBean, N., Fox, A. M., & Litvak, M. E. (2018). Chlorophyll Fluorescence Better Captures Seasonal and Interannual Gross Primary Productivity Dynamics Across Dryland Ecosystems of Southwestern North America. Geophysical Research Letters, 45(2), 748–757. https://doi.org/10.1002/2017GL075922

Stenberg, P. (2007). Simple analytical formula for calculating average photon recollision probability in vegetation canopies. Remote Sensing of Environment, 109(2), 221–224. https://doi.org/10.1016/j.rse.2006.12.014

Stirbet, A. & Govindjee. (2011). On the relation between the Kautsky effect (chlorophyll a fluorescence induction) and Photosystem II: Basics and applications of the OJIP fluorescence transient. Journal of Photochemistry and Photobiology B: Biology, 104(1–2), 236–257. https://doi.org/10.1016/j.jphotobiol.2010.12.010

Stirbet, A., Lazár, D., Guo, Y., & Govindjee, G. (2020). Photosynthesis: Basics, history and modelling. Annals of Botany, 126(4), 511–537. https://doi.org/10.1093/aob/mcz171

Stoy, P. C., El-Madany, T. S., Fisher, J. B., Gentine, P., Gerken, T., Good, S. P., Klosterhalfen, A., Liu, S., Miralles, D. G., Perez-Priego, O., Rigden, A. J., Skaggs, T. H., Wohlfahrt, G., Anderson, R. G., Coenders-Gerrits, A. M. J., Jung, M., Maes, W. H., Mammarella, I., Mauder, M., … Wolf, S. (2019). Reviews and syntheses: Turning the challenges of partitioning ecosystem evaporation and transpiration into opportunities. Biogeosciences, 16(19), 3747–3775. https://doi.org/10.5194/bg-16-3747-2019

Stuckens, J., Verstraeten, W. W., Delalieux, S., Swennen, R., & Coppin, P. (2009). A dorsiventral leaf radiative transfer model: Development, validation and improved model inversion techniques. Remote Sensing of Environment, 113, 2560–2573. https://doi.org/10.1016/j.rse.2009.07.014

Sun, Y., Frankenberg, C., Wood, J. D., Schimel, D. S., Jung, M., Guanter, L., Drewry, D. T., Verma, M., Porcar-Castell, A., Griffis, T. J., Gu, L., Magney, T. S., Köhler, P., Evans, B., & Yuen, K. (2017). OCO-2 advances photosynthesis observation from space via solar-induced chlorophyll fluorescence. Science, 358(6360). https://doi.org/10.1126/SCIENCE.AAM5747/FORMAT/PDF/OEBPS/PAGES/2.PAGE.XHTML

Sun, Y., Wen, J., Gu, L., Joiner, J., Chang, C. Y., Tol, C. V. D., Porcar-Castell, A., Magney, T., Wang, L., Hu, L., Rascher, U., Zarco-Tejada, P., Barrett, C. B., Lai, J., Han, J., & Luo, Z. (2023b). From Remotely-Sensed SIF to Ecosystem Structure, Function, and Service: Part II - Harnessing Data. Global Change Biology. (companion review)

Tcherkez, G., & Limami, A. M. (2019). Net photosynthetic CO2 assimilation: More than just CO2 and O2 reduction cycles. New Phytologist, 223(2), 520–529. https://doi.org/10.1111/NPH.15828

Thum, T., Zaehle, S., Köhler, P., Aalto, T., Aurela, M., Guanter, L., Kolari, P., Laurila, T., Lohila, A., Magnani, F., Tol, C. V. D., & Markkanen, T. (2017). Modelling sun-induced fluorescence and photosynthesis with a land surface model at local and regional scales in northern Europe. Biogeosciences. https://doi.org/10.5194/bg-14-1969-2017

Tietz, S., Hall, C. C., Cruz, J. A., & Kramer, D. M. (2017). NPQ (T): A chlorophyll fluorescence parameter for rapid estimation and imaging of non-photochemical quenching of excitons in photosystem-II-associated antenna complexes. Plant, Cell & Environment, 40(8), 1243–1255. https://doi.org/10.1111/PCE.12924

Tol, C. V. D., Berry, J. A., Campbell, P. K. E., & Rascher, U. (2014). Models of fluorescence and photosynthesis for interpreting measurements of solar-induced chlorophyll fluorescence. Journal of Geophysical Research: Biogeosciences. https://doi.org/10.1002/2014JG002713

Tol, C. van der, Verhoef, W., Timmermans, J., Verhoef, A., & Su, Z. (2009). An integrated model of soil-canopy spectral radiances, photosynthesis, fluorescence, temperature and energy balance. Biogeosciences, 6(12), 3109–3129. https://doi.org/10.5194/bg-6-3109-2009

Tol, C. van der, Vilfan, N., Dauwe, D., Cendrero-Mateo, M. P., & Yang, P. (2019). The scattering and re-absorption of red and near-infrared chlorophyll fluorescence in the models Fluspect and SCOPE. Remote Sensing of Environment, 232, 111292. https://doi.org/10.1016/j.rse.2019.111292

Ustin, S. L., & Jacquemoud, S. (2020). How the optical properties of leaves modify the absorption and scattering of energy and enhance leaf functionality. Remote Sensing of Plant Biodiversity, 349–384. https://doi.org/10.1007/978-3-030-33157-3_14/FIGURES/16

Verhoef, W. (1984). Light scattering by leaf layers with application to canopy reflectance modeling: The SAIL model. Remote Sensing of Environment. https://doi.org/10.1016/0034-4257(84)90057-9

Verhoef, W. (1985). Earth observation modeling based on layer scattering matrices. Remote Sensing of Environment, 17(2), 165–178. https://doi.org/10.1016/0034-4257(85)90072-0

Verhoeven, A. (2014). Sustained energy dissipation in winter evergreens. New Phytologist, 201(1), 57–65. https://doi.org/10.1111/nph.12466

Verrelst, J., Camps-Valls, G., Muñoz-Marí, J., Rivera, J. P., Veroustraete, F., Clevers, J. G. P. W., & Moreno, J. (2015). Optical remote sensing and the retrieval of terrestrial vegetation bio-geophysical properties—A review. ISPRS Journal of Photogrammetry and Remote Sensing, 108, 273–290. https://doi.org/10.1016/j.isprsjprs.2015.05.005

Vilfan, N., Tol, C. V. der, Yang, P., Wyber, R., Malenovský, Z., Robinson, S. A., & Verhoef, W. (2018). Extending Fluspect to simulate xanthophyll driven leaf reflectance dynamics.

Remote Sensing of Environment, 211(April), 345–356. https://doi.org/10.1016/j.rse.2018.04.012

Vilfan, N., Tol, C. van der, Muller, O., Rascher, U., & Verhoef, W. (2016). Fluspect-B: A model for leaf fluorescence, reflectance and transmittance spectra. Remote Sensing of Environment, 186, 596–615. https://doi.org/10.1016/j.rse.2016.09.017

Vogelmann, T. C. (1993). Plant Tissue Optics. Annual Review of Plant Physiology and Plant Molecular Biology, 44(1), 231–251. https://doi.org/10.1146/annurev.pp.44.060193.001311

Wada, M. (2013). Chloroplast movement. Plant Science : An International Journal of Experimental Plant Biology, 210, 177–182. https://doi.org/10.1016/J.PLANTSCI.2013.05.016

Walker, A. P., Johnson, A. L., Rogers, A., Anderson, J., Bridges, R. A., Fisher, R. A., Lu, D., Ricciuto, D. M., Serbin, S. P., & Ye, M. (2021). Multi-hypothesis comparison of Farquhar and Collatz photosynthesis models reveals the unexpected influence of empirical assumptions at leaf and global scales. Global Change Biology, 27(4), 804–822. https://doi.org/10.1111/gcb.15366

Wang, C., Beringer, J., Hutley, L. B., Cleverly, J., Li, J., Liu, Q., & Sun, Y. (2019). Phenology Dynamics of Dryland Ecosystems Along the North Australian Tropical Transect Revealed by Satellite Solar-Induced Chlorophyll Fluorescence. Geophysical Research Letters, 46(10), 5294–5302. https://doi.org/10.1029/2019GL082716

Wang, H., Prentice, I. C., Keenan, T. F., Davis, T. W., Wright, I. J., Cornwell, W. K., Evans, B. J., & Peng, C. (2017). Towards a universal model for carbon dioxide uptake by plants. Nature Plants, 3(9), 734–741. https://doi.org/10.1038/s41477-017-0006-8

Wang, Z., Townsend, P. A., & Kruger, E. L. (2022). Leaf spectroscopy reveals divergent inter- and intra-species foliar trait covariation and trait–environment relationships across NEON domains. New Phytologist. https://doi.org/10.1111/NPH.18204

Way, D. A., & Pearcy, R. W. (2012). Sunflecks in trees and forests: From photosynthetic physiology to global change biology. Tree Physiology, 32(9), 1066–1081. https://doi.org/10.1093/TREEPHYS/TPS064

Wickliff, J. L., & Aronoff, S. (1962). Evidence for Absence of Diurnal Variation of Chlorophyll Content in Mature Leaves of Soybean. Plant Physiology, 37(5), 590. https://doi.org/10.1104/PP.37.5.590

Widlowski, J. L., Mio, C., Disney, M., Adams, J., Andredakis, I., Atzberger, C., Brennan, J., Busetto, L., Chelle, M., Ceccherini, G., Colombo, R., Côté, J. F., Eenmäe, A., Essery, R., Gastellu-Etchegorry, J. P., Gobron, N., Grau, E., Haverd, V., Homolová, L., … Zenone, T. (2015). The fourth phase of the radiative transfer model intercomparison (RAMI) exercise: Actual canopy scenarios and conformity testing. Remote Sensing of Environment, 169, 418–437. https://doi.org/10.1016/J.RSE.2015.08.016

Wittenberghe, S. V., Alonso, L., Verrelst, J., Moreno, J., & Samson, R. (2015). Bidirectional sun-induced chlorophyll fluorescence emission is influenced by leaf structure and light

scattering properties—A bottom-up approach. Remote Sensing of Environment, 158(2015), 169–179. https://doi.org/10.1016/j.rse.2014.11.012

Wullschleger, S. D. (1993). Biochemical Limitations to Carbon Assimilation in C 3 Plants—A Retrospective Analysis of the A/C i Curves from 109 Species. Journal of Experimental Botany, 44(5), 907–920. https://doi.org/10.1093/jxb/44.5.907

Yang, P., Prikaziuk, E., Verhoef, W., & Tol, C. van der. (2021). SCOPE 2.0: A model to simulate vegetated land surface fluxes and satellite signals. Geoscientific Model Development, 14(7), 4697–4712. https://doi.org/10.5194/gmd-14-4697-2021

Yang, P., Tol, C. V. D., Campbell, P. K. E., & Middleton, E. M. (2021). Unraveling the physical and physiological basis for the solar-induced chlorophyll fluorescence and photosynthesis relationship using continuous leaf and canopy measurements of a corn crop. Biogeosciences, 18(2), 441–465. https://doi.org/10.5194/BG-18-441-2021

Yang, P., & Tol, C. van der. (2018). Linking canopy scattering of far-red sun-induced chlorophyll fluorescence with reflectance. Remote Sensing of Environment, 209(February), 456–467. https://doi.org/10.1016/j.rse.2018.02.029

Yang, P., Tol, C. van der, Campbell, P. K. E., & Middleton, E. M. (2020). Fluorescence Correction Vegetation Index (FCVI): A physically based reflectance index to separate physiological and non-physiological information in far-red sun-induced chlorophyll fluorescence. Remote Sensing of Environment, 240, 111676. https://doi.org/10.1016/J.RSE.2020.111676

Yang, P., Tol, C. van der, Verhoef, W., Damm, A., Schickling, A., Kraska, T., Muller, O., & Rascher, U. (2019). Using reflectance to explain vegetation biochemical and structural effects on sun-induced chlorophyll fluorescence. Remote Sensing of Environment, 231(May 2018), 110996. https://doi.org/10.1016/j.rse.2018.11.039

Yang, P., Verhoef, W., & Tol, C. van der. (2017). The mSCOPE model: A simple adaptation to the SCOPE model to describe reflectance, fluorescence and photosynthesis of vertically heterogeneous canopies. Remote Sensing of Environment, 201(March), 1–11. https://doi.org/10.1016/j.rse.2017.08.029

Zaks, J., Amarnath, K., Kramer, D. M., Niyogi, K. K., & Fleming, G. R. (2012). A kinetic model of rapidly reversible nonphotochemical quenching. Proceedings of the National Academy of Sciences of the United States of America, 109(39), 15757–15762. https://doi.org/10.1073/pnas.1211017109

Zarco-Tejada, P. (2005). Development of a Vegetation Fluorescence Canopy Model. ESA Scientific and Technical Publications Branch, April 2005, 1–138.

Zeng, Y., Badgley, G., Chen, M., Li, J., Anderegg, L. D. L., Kornfeld, A., Liu, Q., Xu, B., Yang, B., Yan, K., & Berry, J. A. (2020). A radiative transfer model for solar induced fluorescence using spectral invariants theory. Remote Sensing of Environment, 240(March), 111678. https://doi.org/10.1016/j.rse.2020.111678

Zeng, Y., Badgley, G., Dechant, B., Ryu, Y., Chen, M., & Berry, J. A. (2019). A practical approach for estimating the escape ratio of near-infrared solar-induced chlorophyll

fluorescence. Remote Sensing of Environment, 232(July), 111209. https://doi.org/10.1016/j.rse.2019.05.028

Zhan, W., Yang, X., Ryu, Y., Dechant, B., Huang, Y., Goulas, Y., Kang, M., & Gentine, P. (2022). Two for one: Partitioning CO2 fluxes and understanding the relationship between solar-induced chlorophyll fluorescence and gross primary productivity using machine learning. Agricultural and Forest Meteorology, 321, 108980. https://doi.org/10.1016/J.AGRFORMET.2022.108980

Zhang, Z., Chen, J. M., Guanter, L., He, L., & Zhang, Y. (2019). From Canopy-Leaving to Total Canopy Far-Red Fluorescence Emission for Remote Sensing of Photosynthesis: First Results From TROPOMI. Geophysical Research Letters, 46(21), 12030–12040. https://doi.org/10.1029/2019GL084832

Zhang, Z., Zhang, Y., Porcar-Castell, A., Joiner, J., Guanter, L., Yang, X., Migliavacca, M., Ju, W., Sun, Z., Chen, S., Martini, D., Zhang, Q., Li, Z., Cleverly, J., Wang, H., & Goulas, Y. (2020). Reduction of structural impacts and distinction of photosynthetic pathways in a global estimation of GPP from space-borne solar-induced chlorophyll fluorescence. Remote Sensing of Environment, 240, 111722. https://doi.org/10.1016/j.rse.2020.111722

Zhao, F., Dai, X., Verhoef, W., Guo, Y., Tol, C. van der, Li, Y., & Huang, Y. (2016). FluorWPS: A Monte Carlo ray-tracing model to compute sun-induced chlorophyll fluorescence of three-dimensional canopy. Remote Sensing of Environment, 187, 385–399. https://doi.org/10.1016/j.rse.2016.10.036

Zhou, K., Zhang, Q., Xiong, L., & Gentine, P. (2022). Estimating evapotranspiration using remotely sensed solar-induced fluorescence measurements. Agricultural and Forest Meteorology, 314, 108800. https://doi.org/10.1016/j.agrformet.2021.108800